FINAL REPORT

LIGHT FUNNEL CONCENTRATOR PANEL FOR SOLAR POWER

Contract #NAS8-36463

D180-30473-1

Submitted to

NASA
MARSHALL SPACE FLIGHT CENTER
Huntsville, Alabama

MAY 1987

(NASA-CR-179223) LIGHT FUNNEL CONCENTRATOR PANEL FOR SOLAR POWER Final Report (Boeing Aerospace Co.) 60 p CSCL 10B

N88-12870

Unclas
G3/44 0109774

Boeing Aerospace Company
Seattle, Washington 98124

TABLE OF CONTENTS

TABLE OF CONTENTS (Continued)

LIST OF FIGURES

LIST OF FIGURES (Continued)

LIST OF TABLES

SECTION 1.0
INTRODUCTION

The program reported herein involves a new concept in solar concentrator design. The concept provides a theoretical concentration efficiency of 96% with power-to-weight ratios as high as 50 W/kg. Further, it eliminates the need for fragile reflective coatings and is very tolerant to pointing inaccuracies.

The concept differs from conventional reflective mirrors and lens designs in that it uses the principle of total internal reflection in order to funnel incident sunlight into a concentrator photovoltaic cell. Thus, the concept is appropriately called the light funnel concentrator and appears to be a significant improvement over conventional concepts for concentrating space power systems.

SECTION 2.0

DESCRIPTION OF PROGRAM

The focus of this program deals with the detailed optical/electrical, mechanical, thermal, and structural analysis of the concept and the development of component fabrication techniques with which to generate test articles for experimentally establishing feasibility of the concept.

2.1 SCOPE OF PROGRAM

Figure 2-1 shows a task-flow diagram used to determine the feasibility of the light funnel concentrator concept through a balanced approach of analysis, development and fabrication of prototypes, and testing of components. A three-dimensional optical model of the light funnel concentrator and photovoltaic cell was developed in order to assess the ultimate performance of such systems. In addition, a thermal and structural analysis of a typical unit was made.

Techniques of (1) fabricating the light funnel cones, (2) optically coupling them to GaAs concentrator cells, (3) bonding the funnels to GaAs cells, (4) making electrical interconnects, and (5) bonding substrates was explored and a prototype light funnel concentrator unit was fabricated and tested. Testing of the system included measurements of optical concentrating efficiency, optical concentrator to cell coupling efficiency, and electrical efficiency.

2.2 CONCEPT DESCRIPTION

2.2.1 Physical Principle

The light funnel concentrator concept differs from conventional reflective mirrors and lens designs in that it uses the principle of total internal reflection in order to direct incident sunlight into a concentrator cell. A cross-section of an internal reflection concentrator segment is shown in figure 2-2. In principle, light entering the front surface of the structure is trapped by internal reflection and funneled down to the exit where a concentrated spot of highly diffuse light results.

2.2.2 Physical Geometry

The critical parameters of the light funnel identified in figure 2-2 are the angles θ and β. For a given angle θ, which is chosen by a trade between its angular dependent surface reflectance and system weight will be discussed later, β must be chosen, based on the index of refraction of the material so that light incident parallel to the optical axis will encounter the rear surface at an angle equal to or greater than the critical angle so that the total internal reflection occurs. Each succeeding reflection then becomes farther from the critical angle allowing the light to totally reflect until it strikes the base of the funnel. The light is incident on the base of the funnel with a wide range of angles. If the emergent medium is air or vacuum, total internal reflection will occur for base incident angles greater than 42 degrees regardless of any AR-coatings applied, and high reflection occurs at angles near the critical angle. When the light is optically coupled to a higher refractive index solar cell, with intermediate index antireflective coatings and adhesive, total internal reflection does not occur at the base, and the base reflection can be reduced to very low values.

2.2.3 Theoretical Efficiency

In theory, the light funnel can be made better than 96% efficient for concentrating that portion of the AMO solar spectrum that is in-band for silicon or GaAs photovoltaic cells. Figure 2-3 shows the transmittance of fused silica compared to the energy spectrum of AMO sunlight.

Basically, the only losses are due to reflection at the interfaces of the glass. These losses are about 4% at each interface for normally incident light on glass in air or vacuum. These losses can be reduced to 1.5% or less by adding a coating with an intermediate index of refraction. As the angle of incidence varies from normal, the reflection losses increase. For example, borosilicate glass will reflect about 17% of the light incident at 70 degrees with respect to the normal to its surface (θ = 20 deg in fig. 2-2). However, the absolute reflectance and the angular dependence can be reduced by the addition of AR-coatings so that the maximum concentrating efficiency of the light funnel concentrator is greater than 96%.

2.2.4 Concentration Characterisics

The theoretical concentration ratio, C_R, is defined by the ratio of the area of the cone aperture (collecting area) to the area of the cone base (emitting area). Mathematically, this ratio can be expressed by the relationship

$$C_R = \left(\frac{\tan\theta}{\tan\theta - \tan\beta} \right)^2$$

if the inner cone apex lies on the base plane. Figure 2-4 shows the functional dependence of C_R and angle θ, when β is set at the critical angle. Thus, from a concentration ratio consideration, it is desirable to use as small an angle θ as is practical.

2.2.5 Light Collection Optimization

The practical lower limit for θ is determined by the light collection efficiency of the funnel. In order for the light funnel to function, the incident light must penetrate into the glass material. Figure 2-5 shows the angular dependence of reflectance for the case of bare fused silica. As can be seen from the curve, the reflectance of the fused silica surface begins increasing as the angle, θ, decreases. Based on consideration of concentration ratio and reflectance, a value for θ of approximately 20 degrees is optimum.

The reflection losses at shallow angles can be greatly reduced by the addition of an AR-coating having an index of refraction intermediate between that of vacuum and fused silica with its thickness one-fourth wavelength matched to a wavelength near the peak of the air mass zero (AMO) spectrum incident at 20 degrees with respect to the concentrator surface.

2.2.6 Optical Matching to Photovoltaic Cells

Another requirement for efficient operation of the light funnel concentrator is that it be able to deliver the concentrated photons to the photovoltaic cells. The photons strike the base of the funnel over a wide range of angles. In order to maximize the number of photons penetrating the photovoltaic cells, the surface of the cell must be optically matched to the base of the light funnel at the average angle that the photons strike the surface. In order to determine the appropriate matching medium, the photon exit angle distribution must be analyzed and the cell material must be selected. In order to determine these angles and make a material selection, it will be necessary to develop a three-dimensional ray tracing model for the light funnel.

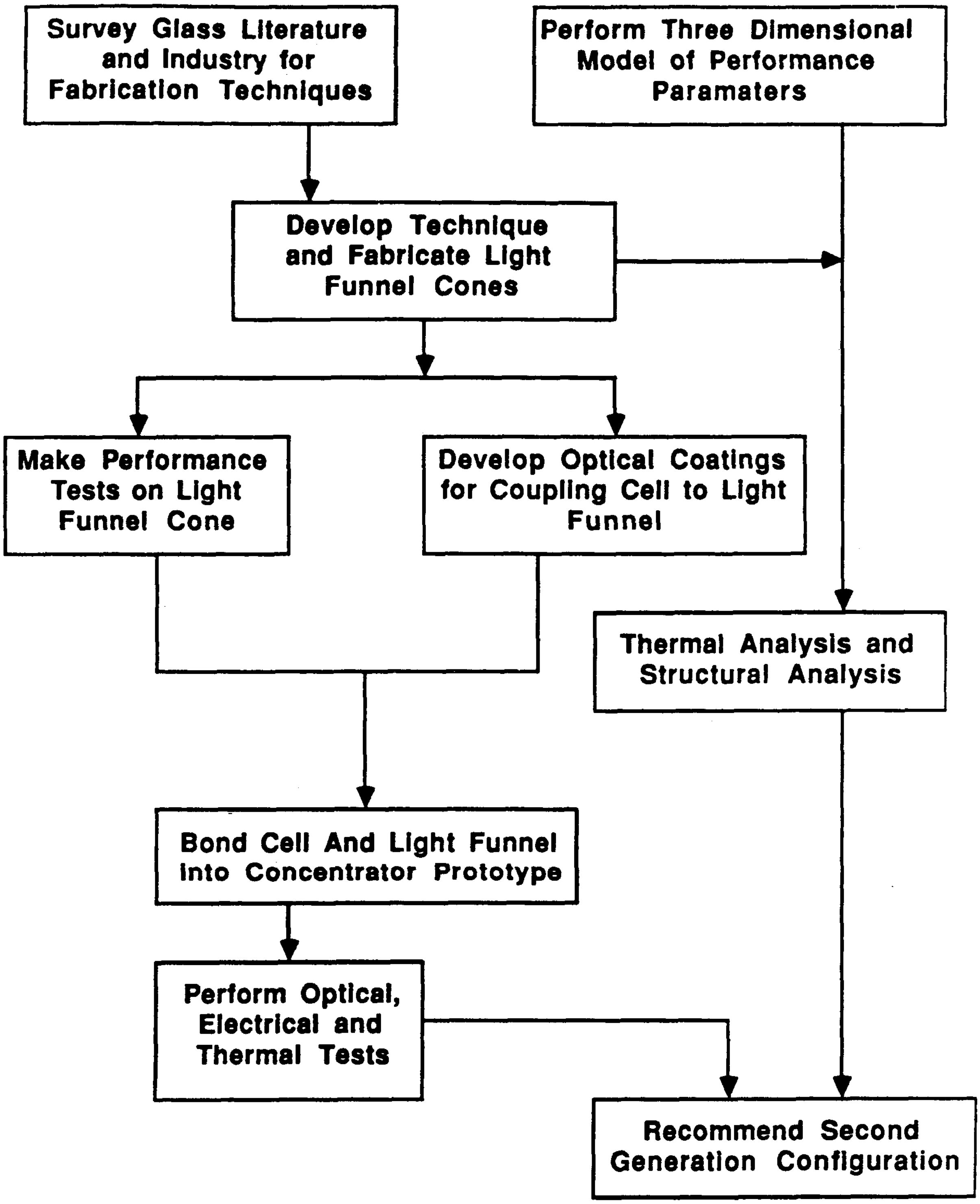

Figure 2-1. Flow Diagram of Developmental Effort

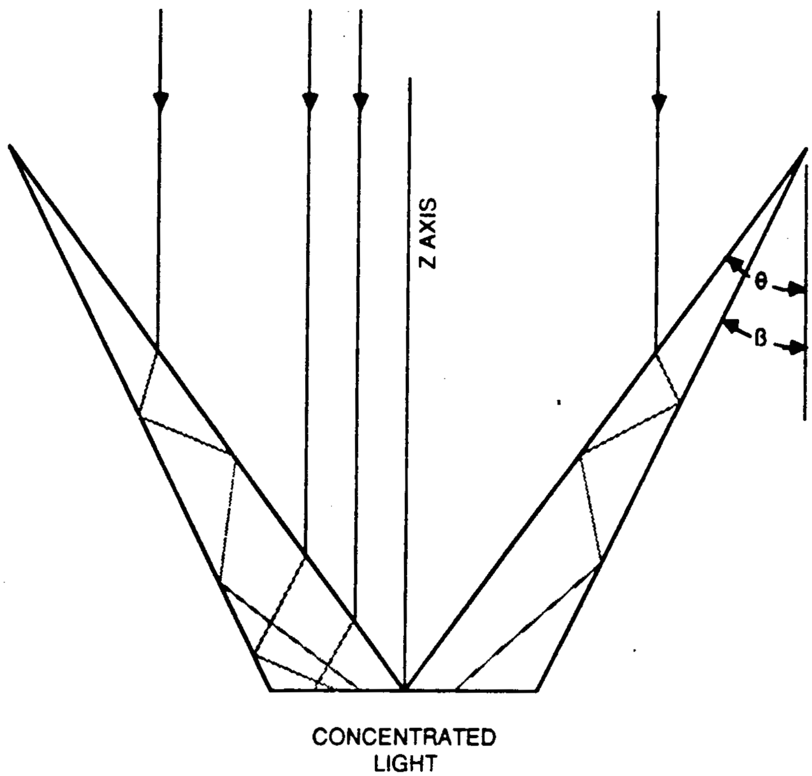

Figure 2-2. Illustration of Light Funnel Concentrator Concept

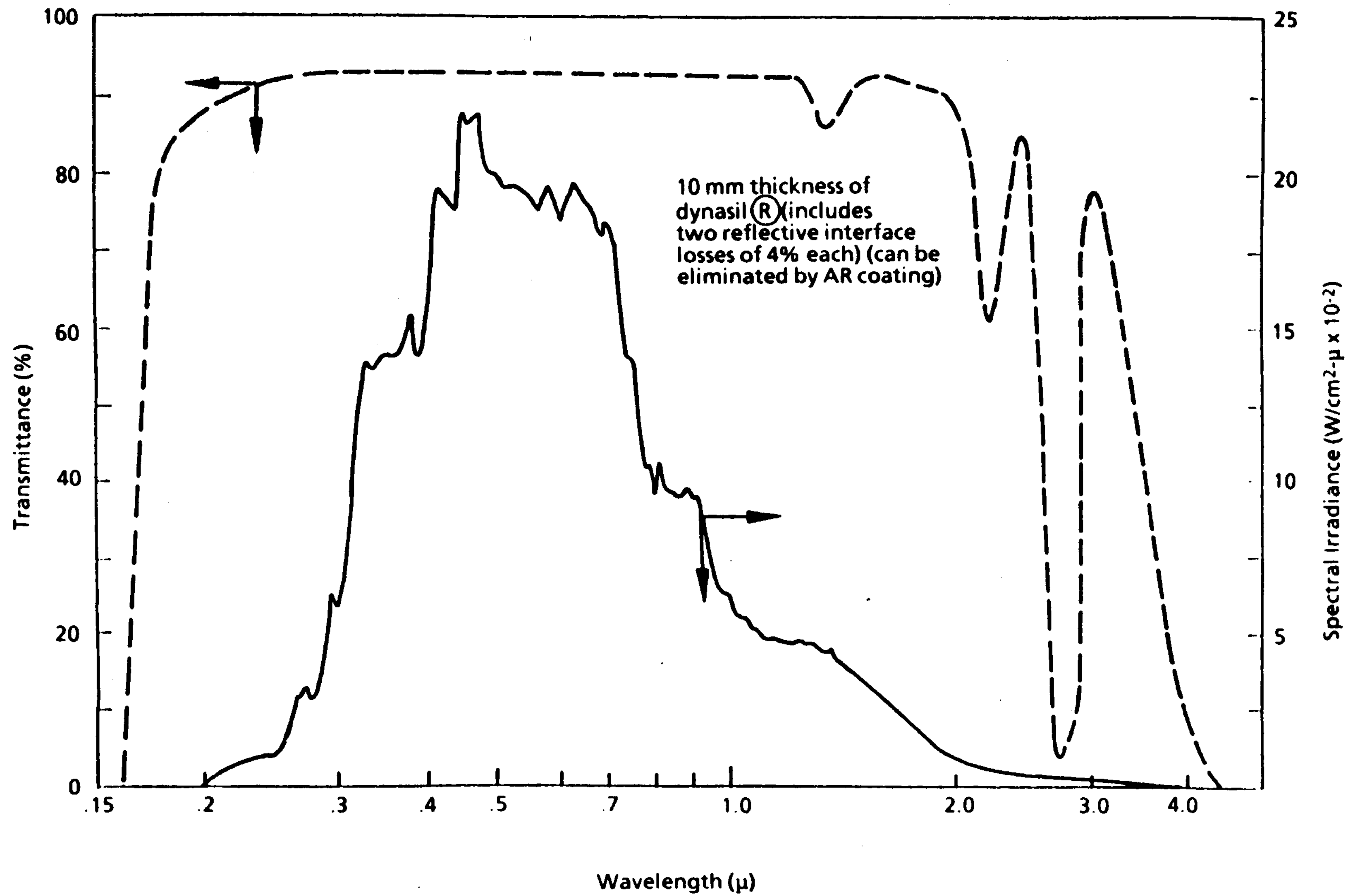

Figure 2-3. Comparison of Dynasil Fused Silica Transmittance With Air Mass Zero Solar Irradiance Spectrum

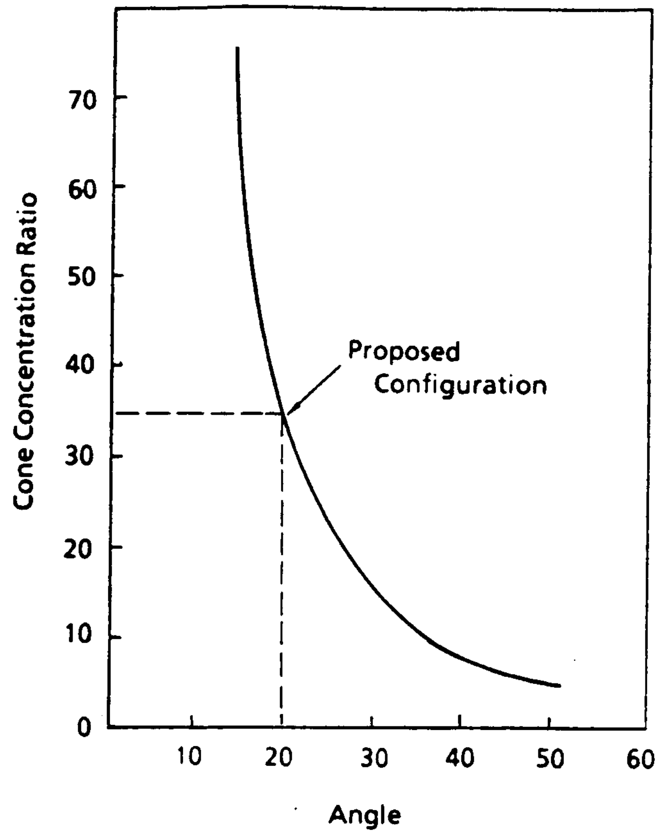

Figure 2-4. Concentration Ratio for Conical Light Funnel Versus Angle of InnerSurface Relative to Optical Axis

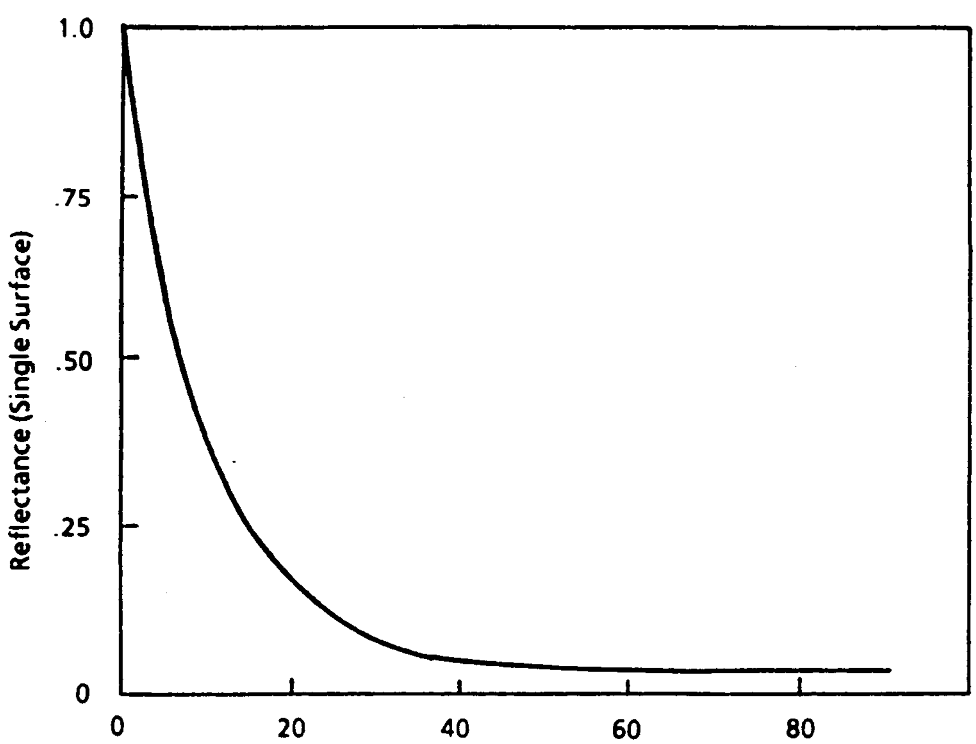

Figure 2-5. Angular Dependence of Surface Reflectance for Fused Silica With Respect to Optical Axis of Light Funnel

SECTION 3.0

LIGHT FUNNEL MODELING

A cross-section of an internal reflection segment of a light funnel is shown in figure 2-2. Light entering the front (or inner) surface of the glass structure is trapped by internal reflection and funneled to the exit where a concentrated spot of highly diffuse light results. The critical parameters are the angles θ and β. For a given θ, β must be chosen, based on the refractive index of the material so that light incident parallel to the optical axis will encounter the rear surface at angle equal to or greater than the critical angle, so that total internal reflection occurs. Each succeeding reflection then becomes farther from the critical angle, allowing the light to totally reflect until it strikes the end of the funnel. At the end of the funnel the light will strike at various angles. An antireflective coating is designed to allow the least amount of attenuation as this light passes from the glass to the GaAs solar cell.

An existing three-dimensional ray-tracing code was used to evaluate the light funnel configuration and determine pointing angle sensitivity. The code was modified to allow examination of the exit angles of the rays at the bottom of the funnel. The code assumes parallel rays input at various incoming angles.

The ray-tracing code development started with defining the equations of the primary and secondary surfaces of the concentrator material. The equations were then solved for the intersection of the incident ray line and the primary surface. The angle made between this line and the normal to the surface was then found and appropriate laws of optics were applied to find the fraction of energy in the ray which was refracted into the concentrator material and the direction in space of this refracted ray. An equation for a new line was then defined from this direction and the primary intersection point. Then, the intersection and angle of the new line and the secondary surface was found and the angle was compared with the critical angle for internal reflection. If the angle was less than the critical angle or some reasonable fraction thereof, the ray was assumed to escape the concentrator; if not, the ray was assumed to be trapped. The above ray process was repeated following the ray from the secondary surface back to the primary and so on down to the bottom plane. The ray was then checked to see if it intersected the bottom plane at less than the critical angle.

3.1 LIGHT FUNNEL DESIGN

Various funnel designs were investigated and refined to optimize funnel performance and producibility. Module assembly parameters and procedures, as well as matching to the energy-converison cell also being selected, were considered in designing the optimized light funnel. The results of this effort are shown in figure 3-1.

Figure 3-1 was developed based on a cell size of 0.4-cm diameter. This cell size was used since GaAs cells of this size are commercially available. A concentration ratio of 35 was the other major constraint on the design.

Given these constraints, the top inside radius was set to 1.15 cm and the top outside radius was set to 1.2 cm. The difference in inside and outside radii is due to manufacturing difficulties associated with a knife edge. The height was determined by the relationship of the angles θ and β. The angle θ was chosen to be 20 degrees as discussed in section 2.2.5. The angle β was then varied and the three-dimensional code used to determine efficiency and pointing angle tolerance. Figure 3-2 shows the result of this study for this configuration. As a result of this study, β was chosen to be 16.5 degrees as a starting point for the design.

The next step was to determine a height and a depth between the inside point of the funnel and the bottom of the funnel. This height needs to be a dimension that can be used in manufacturing, unlike the angles θ and β. Therefore these dimensions were determined using the angles calculated above and then refined to dimensions suitable for a manufacturing drawing. The height of the funnel was determined to be 3.36 cm and the depth of the inside of the funnel 3.15 cm. The angles θ and β were then recalculated using these new dimensions and found to be 20 degrees and 16.6 degrees, respectively.

The three-dimensional code was then used to evaluate this design for efficiency and pointing angle tolerance. The results are shown in figure 3-3. A plot of the rays, as they pass through a plane of the light funnel concentrator, is shown in figure 3-4. This figure shows the major difficulty in this design. When the point of the inner cone does not reach the bottom of the funnel this allows rays to pass from one outside wall to the other, missing the inner surface. If the bottom is close enough to the inner point, the rays hit the bottom before reaching the opposite side of the outer cone. If the rays do reach the opposite side of the outer cone, they escape when they hit this surface as they are now at less than the critical angle for total reflection. This explains why the pointing angle tolerance shown in figure 3-2 falls off after β decreases past a certain point. The smaller β is the more gap there will be at the bottom of the funnel and the more rays will escape.

Figure 3-5 shows the distribution of rays hitting the bottom of the funnel based on incoming rays spaced radially every 22.5 degrees around the top of the funnel. The exit angles were recalculated and the results can be seen in the histogram in figure 3-6. The average exit angle is about 25 degrees and the antireflection filter was designed for this angle.

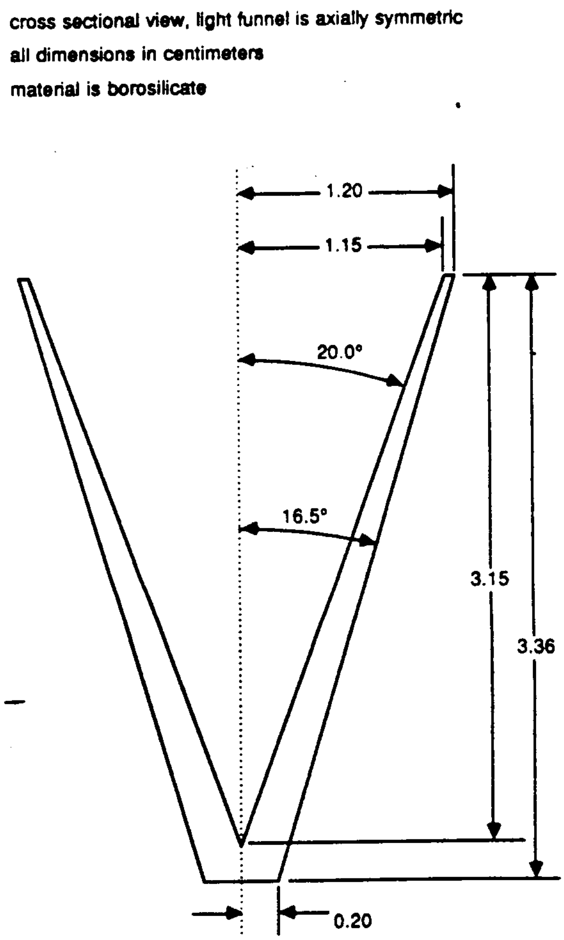

Figure 3-1. Light Funnel Concentrator

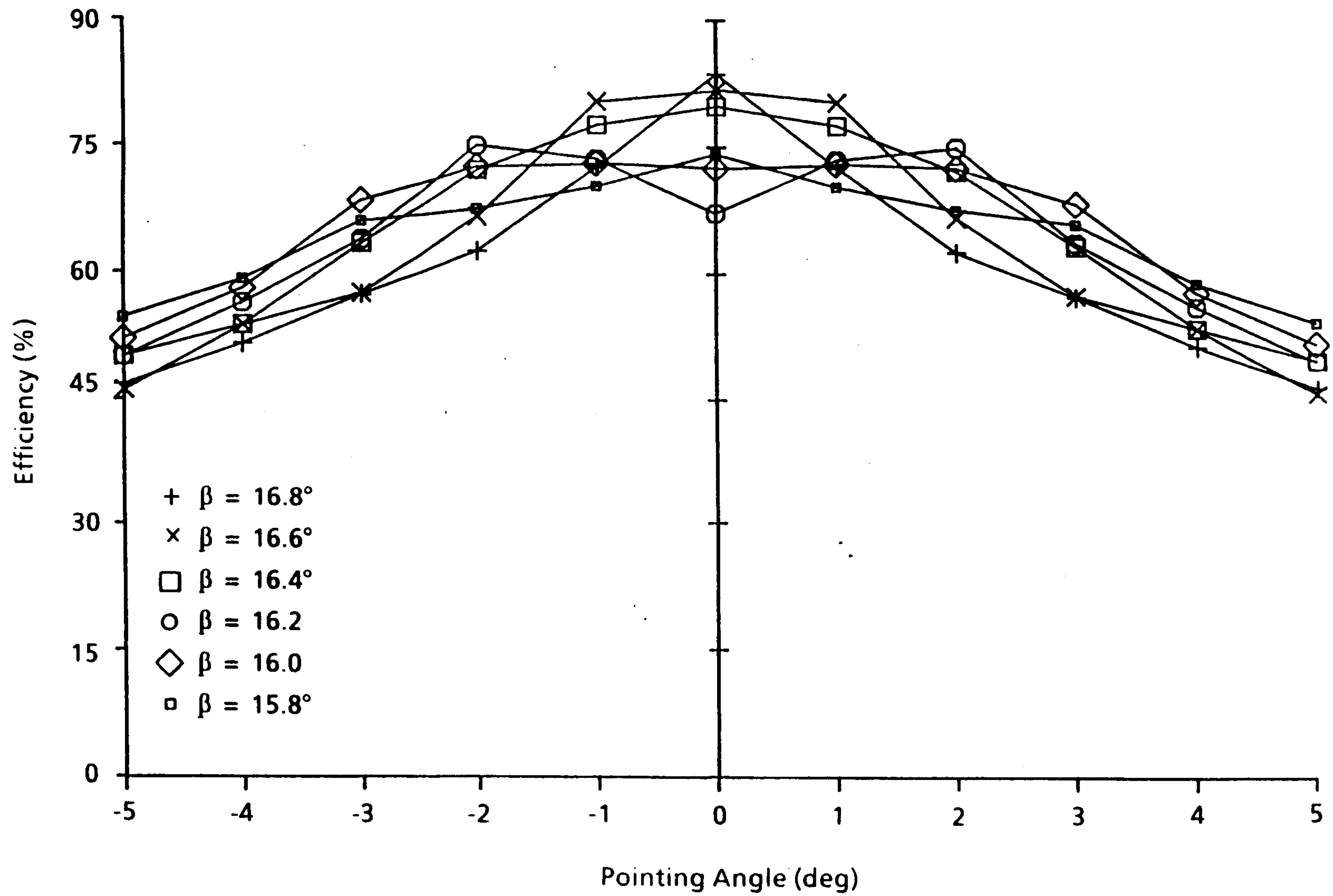

Figure 3-2. Plot of Pointing Angle Tolerance for Various Values of Beta

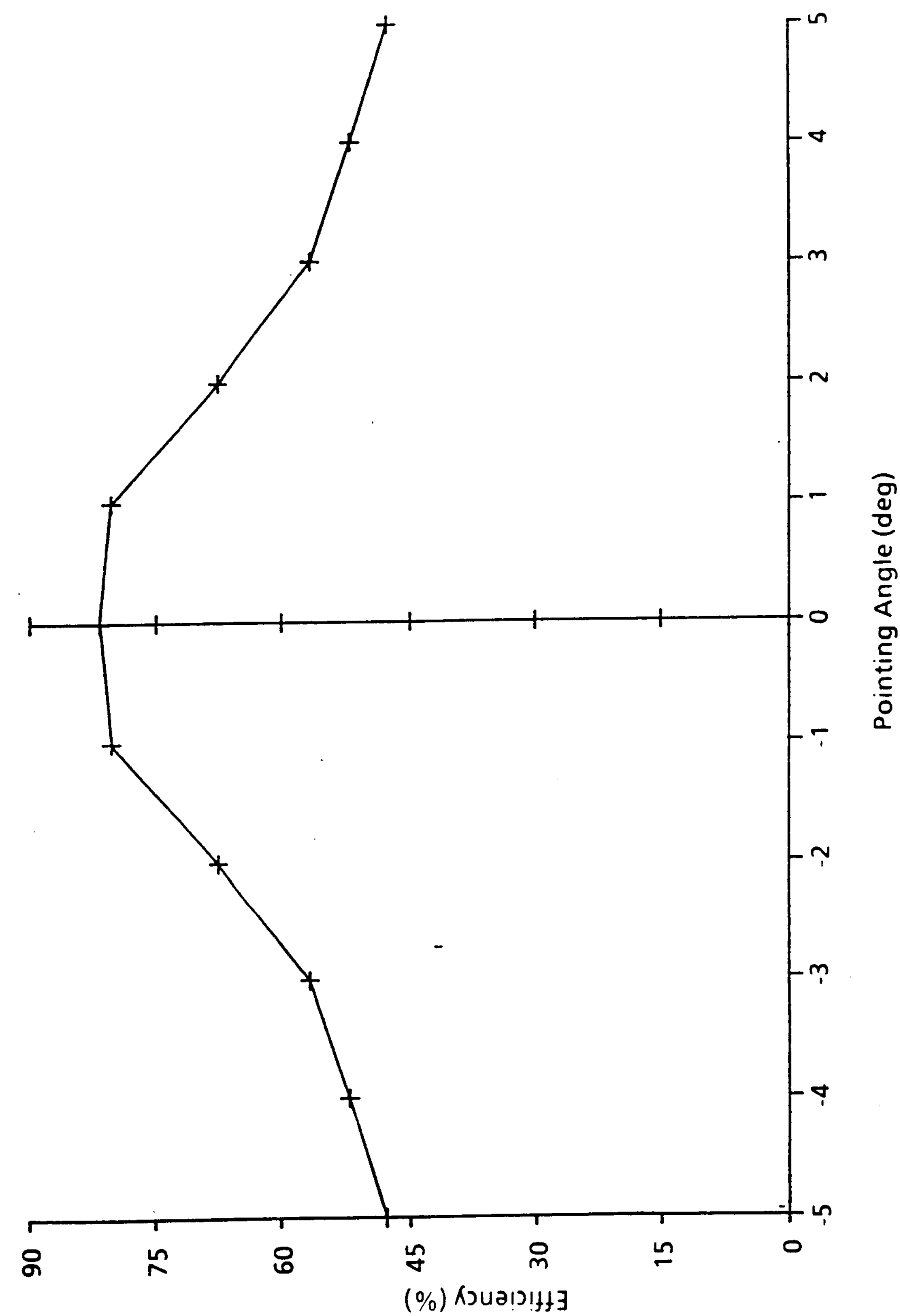

Figure 3-3. Pointing Angle Tolerance for Beta = 16.574 Degrees

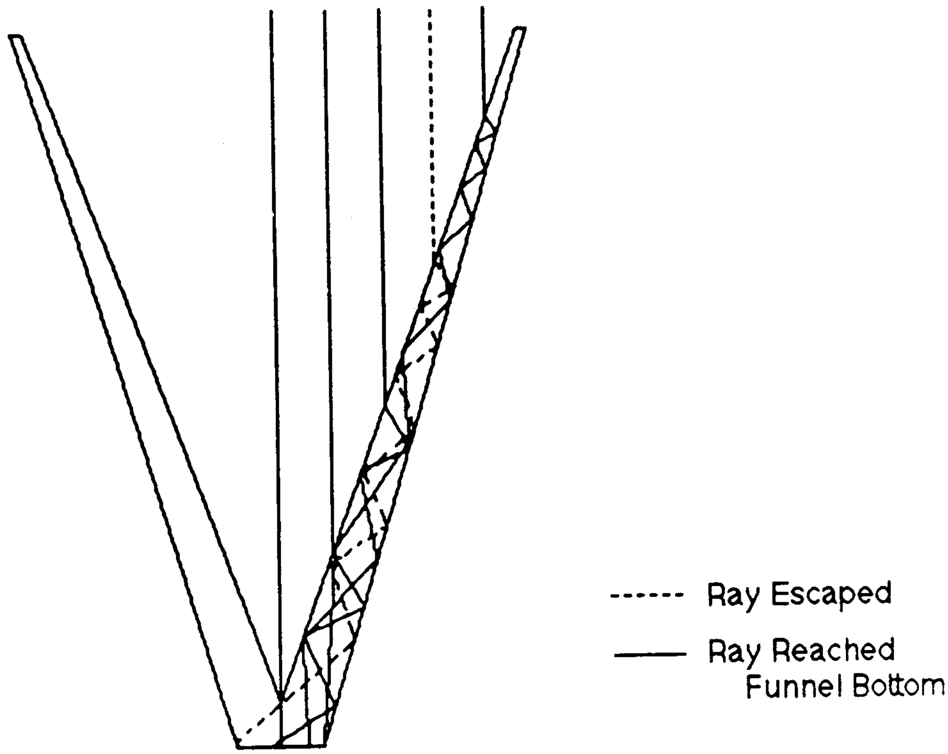

Figure 3-4. Ray Trace Through a Plane of the Light Funnel Concentrator

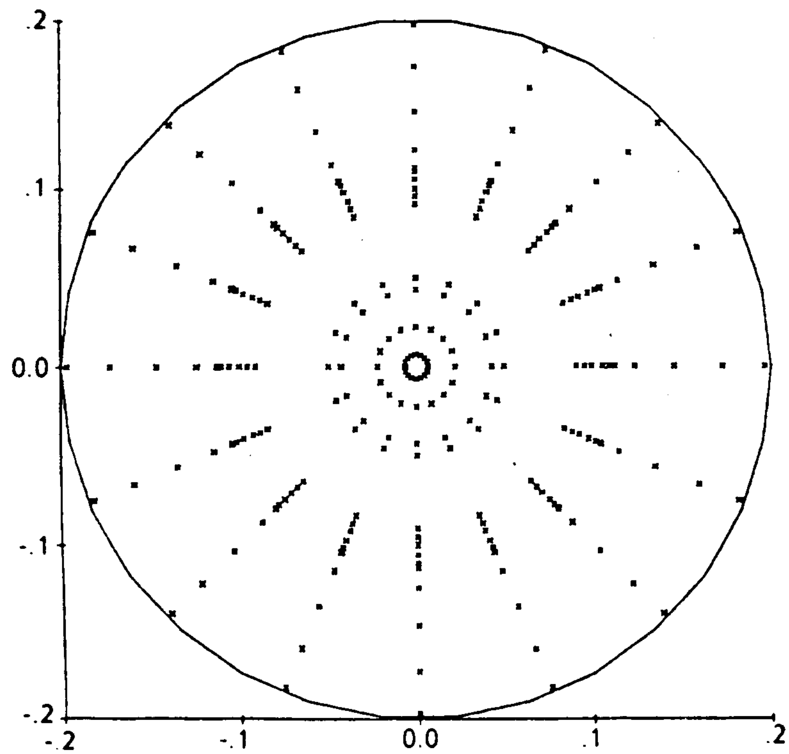

Figure 3-5. Distribution of Rays Hitting the Bottom of the Light Funnel Concentrator

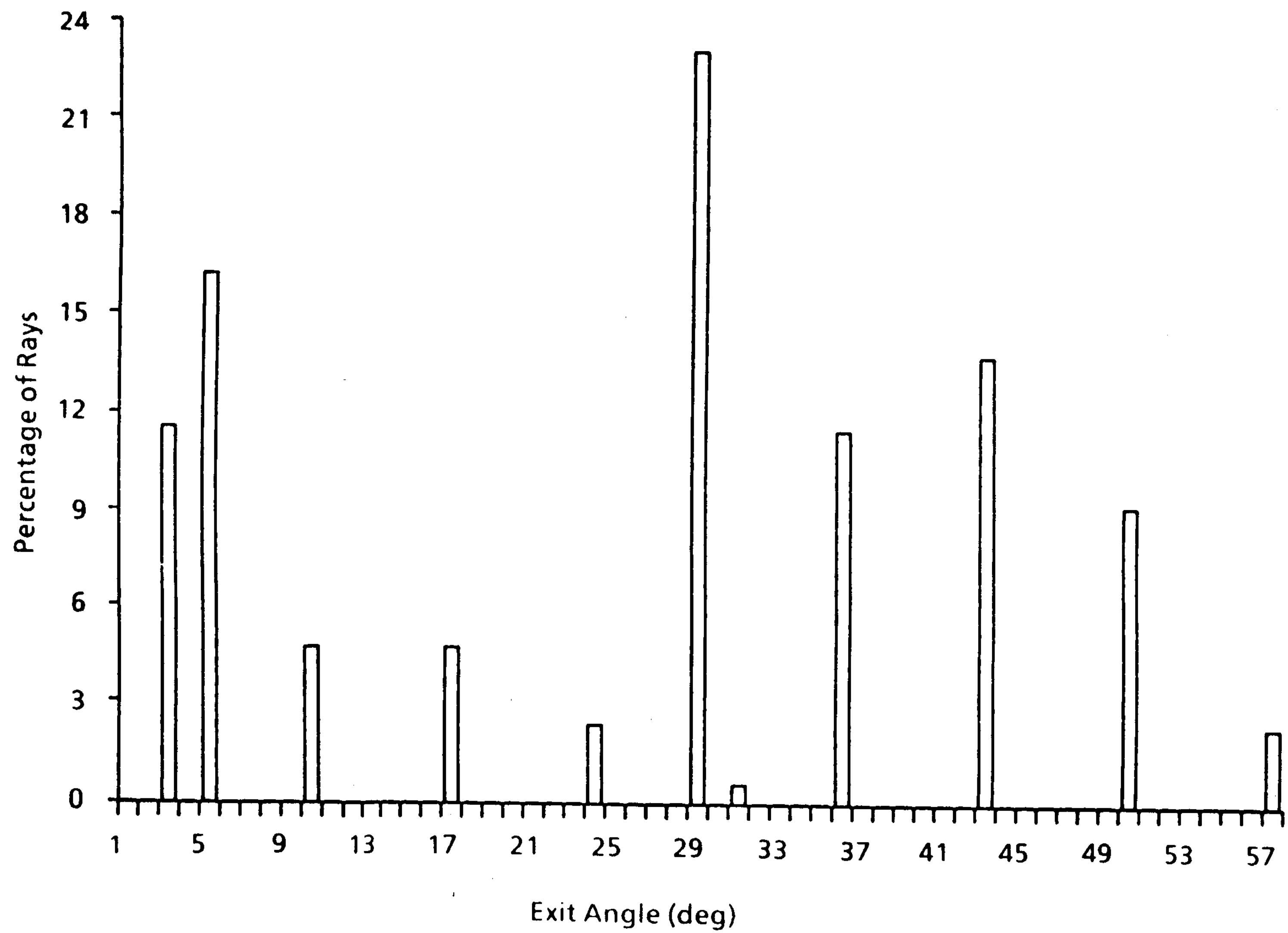

Figure 3-6. Distribution of Exit Angles

SECTION 4.0

FABRICATION OF LIGHT FUNNELS

4.1 SURVEY OF GLASS INDUSTRY AND RELATED LITERATURE

A literature search was conducted of COMPENDEX and DIALOG files for publications pertaining to glass molding. Some applicable articles were identified and requested. Several more glass equipment manufacturing firms were contacted to investigate the cost and availability of purchasing glass molding apparatus. Costs and schedules for these alternatives were found excessive for the scope of this contract.

The possibility of forming light funnels in existing hot press machines in Boeing's Materials and Processes Laboratories was investigated. Candidate forming methods, included hot isostatic pressing (HIP) and hot pressing in an inert gas medium. There is experience in forming glasses and ceramics in HIP process, but the extremely high-forming operation cost appears prohibitive. Vendors outside of Boeing were contacted about custom molding the light funnels from borosilicate glass. Weiss Scientific Glass appeared to have the best processes.

SECTION 5.0

LIGHT FUNNEL ANTIREFLECTIVE COATING DESIGN

Antireflective (AR) coatings were designed to increase the light transmittance into the light funnels through the inner cone surface, and out of the light funnel through the base plane.

The AR-coating design for the inside cone surface entailed the use of a single-layer MgF_2 coating. A single-layer AR-coating was chosen due to its improved transmittance over a broad wavelength range, wide tolerance in coating thickness with little performance penalty, relative economy, and ease of application when compared to multilayer coatings.

A well-designed multilayer AR-coating has the advantage of offering very low reflectance over a well-defined and relatively broad passband. However, outside the passband wavelength range, the coating reflectance becomes significantly higher than the uncoated funnel. A single-layer AR-coating is never more reflective than the uncoated substrate (see figs. 5-1 and 5-2).

The thickness accuracy required for a multilayer AR-coating was beyond the capabilities of any local coating facility investigated. Due to the large aspect ratio of the inside cone, there is a high degree of uncertainty of the actual coating on the light funnels when compared to a normal flat witness substrate. Additionally, if one has more than one deposition source, any misalignment with the cone axis will result in poor uniformity around the cone inner surface of the various coating materials.

When designing a single-layer AR-coating, the optimum coating causes 180 degrees out of phase interference between the light reflected from the first surface (air/AR-coating interface) and the second surface (AR-coating/substrate interface). The coating material determines the reflection amplitudes at the two surfaces, with the ideal coating causing the reflected light from the two interfaces to completely cancel, yielding zero reflectivity. The reflectivity formulas used for single-layer AR-coatings are as follows:

$$R = \frac{r_1^2 + r_2^2 - 2\, r_1\, r_2 \cos \delta}{1 + r_1^2\, r_2^2 - 2\, r_1\, r_2 \cos \delta}$$

where r_1 = first surface reflectivity

r_2 = second surface reflectivity

δ = phase difference in reflected light

when $\delta = \pi$, the reflection is minimized:

$$R_{min} = \frac{\left(r_1 + r_2\right)^2}{\left(1 + r_1 r_2\right)^2} \tag{1}$$

The optimum reflectivity values for a single-layer AR-coating are attained when the AR film index of refraction has a value

$$\text{optimum } n_f = \sqrt{n_o n_s} \tag{2}$$

where n_f = AR film refractive index

n_o = incident medium refractive index

n_s = substrate refractive index

for a borosilicate light funnel in air or vacuum,

$n_s = 1.5$ $\qquad$ $n_o = 100$

yielding: optimum $n_f = 1.22$

Magnesium fluoride (MgF_2) has the lowest refractive index value ($n = 1.38$) of all the materials which form a durable coating on glass.

At near normal light incidence, a quarter-wavelength optical thickness (QWOT) AR-coating of MgF_2 on borosilicate glass will reduce surface reflection from approximately 4% to 1.5%.

At large angles of light incidence with respect to normal, the S-polarized radiation is reflected with a different functional relation than the P-polarization, and the phase difference in reflected light has a complex form. The equations for the parameters used in preceding equations (1) and (2) are as follows:

$$R = \frac{1}{2}\left(R_s + R_p\right) \tag{3}$$

$$-r_{s1} = \frac{n_0 \cos \theta_0 - n_1 \cos \theta_1}{n_0 \cos \theta_0 + n_1 \cos \theta_1} \tag{4}$$

$$r_{s2} = \frac{n_1 \cos \theta_1 - n_2 \cos \theta_2}{n_1 \cos \theta_1 + n_2 \cos \theta_2}$$

$$-r_{p1} = \frac{\dfrac{n_0}{\cos \theta_0} - \dfrac{n_1}{\cos \theta_1}}{\dfrac{n_0}{\cos \theta_0} + \dfrac{n_1}{\cos \theta_1}}$$

$$-r_{p2} = \frac{\dfrac{n_1}{\cos \theta_1} - \dfrac{n_2}{\cos \theta_2}}{\dfrac{n_1}{\cos \theta_1} + \dfrac{n_2}{\cos \theta_2}}$$

Snell's law $n_0 \sin \theta_0 = n_1 \sin \theta_1 = n_2 \sin \theta_2$ (5)

Phase difference $\delta = \frac{4\pi}{\lambda} t\, n_1 \cos \theta_1$

where τ = AR film thickness

λ = incident radiation wavelength

At the 70 degrees incident light angle (θ_0) design for the light funnel inner cone, the reflection from uncoated borosilicate glass is approximately 17%. An optimum coating of MgF_2 can reduce this to 12%. Lower reflection values can be obtained with a coating of lower effective index of refraction, which can be produced with multilayered coatings.

5.1 BASE AR-COATING DESIGN

Antireflective coatings were designed for the light funnel base surface to meet two requirements:

1) low reflection optical coupling into GaAs solar cells, and
2) reduce base reflection in light funnel performance tests with air as the emergent medium.

To meet these objectives, separate coatings were designed for the light funnel and the GaAs solar cells.

5.1.1 GaAs Cell Optical Coupling

The AR-coating on the GaAs concentrator solar cells is plasma-deposited amorphous hydrogenated silicon nitride (α - ω_{ix} Ny:H), with an index of refraction of approximately 2.1, and a thickness of one quarter-wave optical thickness (QWOT) at 650 nm. This coating was applied by the cell manufacturer, the Kopin Company, in a cooperative solar cell development program with Boeing. When the light funnels are tested in a module configuration with the GaAs concentrator cells, Dow Corning 93500 space-grade encapsulant is used to optically couple the light funnel to the solar cell. The index of refraction of the DC-93500 is approximately 1.4 for the visible spectrum. This index of refraction is close to the index of the light funnel (n = 1.5) and very little light reflects from the funnel and DC-93500 interface. For normal incidence, the reflection intensity from this interface is approximately 0.1%. At this interface the critical angle is 70 degrees, which is greater than any of the predicted ray angles incident on the light funnel base, so total internal reflection does not occur for any predicted light rays.

The optimum single-layer AR-coating between the DC-93500 and the GaAs solar cell would have an index of refraction of approximately 2.2, where

$$n_{opt} = \sqrt{n_{DC\text{-}93500} \cdot n_{GaAs}}$$

$$= \sqrt{1.41 \cdot 3.5} = 2.2$$

The AR-coating on the cell has an index of refraction very close to this value (n = 2.1), and is near ideal for use with the light funnel concentrator.

5.1.2 Base Coating for Integrating Sphere Tests

The investigation of light funnel performance independent of solar cell response involved using an integrating sphere apparatus to measure the light throughput of the light funnels as a function of pointing angle. In this test fixture, the light emerges from the light funnel base into air, with a step in index of refraction from n = 1.5 in the glass to n = 1.0 in air. The large transition in index of refraction at this interface causes significant reflection due to the large angle of incidence of much of the light at this surface. Figure 3-6 illustrates the distribution of light ray incident angles with respect to the base normal, as predicted by the light funnel computer model ray tracing code. Any rays that intercept the base at angles greater than the critical angle, θ_C = 41.8 degrees, will be totally reflected back up the cone. These rays account for more than 25% of the total light incident on the funnel base, as modeled by the ray tracing code, and cannot be recovered with any antireflective coating. Light that intercepts the base at angles close to the critical angle will also have a high degree of reflection, but this can be reduced with the appropriate AR-coating.

The light not totally reflected has an average 18 degrees incident angle with the base normal. A single-layer magnesium fluoride AR-coating was designed for the 18 degrees off-normal case, with a specified thickness of 1.05 KA. For the average incident angle of 18 degrees, the AR-coating would reduce base reflection from approximately 4% to 1.5%. However, in the ray tracing model, the base angle of incidence varies from about 3 degrees to 51 degrees, with the resulting reflection with the AR-coating varying from 1.5% to 100%. The actual funnel dimensional variation would significantly alter the base angle distribution. The index of refraction of magnesium fluoride (n = 1.38) is very close to that of the DC-93500 adhesive (n = 1.41) used to bond the light funnel to the GaAs solar cell. As a result, a light funnel with a MgF_2 base AR-coating should not appreciably change the performance of a light funnel and GaAs module.

SECTION 6.0

MODULE DESIGN

An array of seven funnel and cell units was assembled to evaluate bonding schemes and provide a module for structural testing. A unit consisted of a light funnel and GaAs concentrator cell bonded together with DC-93500. The funnels were faceted at the top to form a hexagon. Individual units were assembled into a module by bonding the funnels together at the faceted surfaces with DC-93500. The cells were bonded to a common substrate using RTV 566A. Figure 6-1 is a photograph of the completed assembly.

6.1 SPECTRAL RESPONSE OF CONCENTRATOR CELLS

The spectral response of a GaAs concentrator cell is presented in figure 6-2 and table 6-1. A schematic diagram of the measurement system is shown in figure 6-3. Light from a dc-powered tungsten source passes through a monochromator with two interchangeable gratings and a collimating lens and is intercepted by a light-chopping blade placed at 45 degrees to the path of the incoming light beam. The transmitted beam illuminates the cell under test. The beam reflected from the chopper is monitored by a calibrated photovoltaic detector (either Si or Ge) to give a continuous measurement of the light intensity. All controls as well as data acquisitions and calculations are provided by a process measurement controller and a H-P desk computer. The system can measure the cell response within the wavelength range from 440 nm to 1800 nm. Typically, the cell spectra responsibility (A/W) and quantum efficiency (electrons/photons) are measured from 450 nm to 1400 nm. Integration of the measured cell responsibility over a AMI solar spectrum can be performed by the computer to compare the short circuit current to the measured I_{SC} under ELH lamp.

6.2 ANGULAR DEPENDENCE OF CELL OUTPUT

Figure 3-6 in section 3.1 provides the angular distribution of light exiting the light funnel. Since the concentrator cell receives light over this broad angular range, it is necessary to measure the cell angular response to predict the collection efficiency of the cell.

To provide this information, a fixture was fabricated to allow measurement of cell short-circuit voltage as a function of incident light angle. A (0.63 microns) with a nominal 1 mm diameter beam was used for the light source and a 5 mm diameter (active region) GaAs concentrator cell from Kopin was used for the test sample. Figure 6-4 shows the results over the incident angular range from normal to 70 degrees. Two factors affect the interpretation of these data. The active cell region is circular and divided into four quadrants with respect to cell pickup-bar geometry. Bars in each quadrant run perpendicular to those in adjacent quadrants. As the angle of incidence varies from 0 degree to 70 degrees off-normal, the "footprint" of the beam on the cell changes from 1 mm circular to 1 mm x 3 mm oblong. To minimize the effects of pickup-bar influence on the data, the cell was "scanned" across two quadrants on a line tangent to approximately one-half the radius of the active region. A centerline "scan" was also made to determine the influence of a constantly present pickup bar. The two factors are thus the contribution of the pickup bar on the illuminated area for the normal incidence case and the total relative contribution for the off-normal cases. Figure 6-4 provides data from a centerline "scan" and a left-and-right-of-center "scan". As expected, the centerline data is lowest due to the constant presence of a pickup bar in the illuminated area. An average of the right and left "scans" should provide the most usable information. The "scan" paths are shown in figure 6-4. In actuality the HeNe beam, at normal incidence, is placed near the lower edge of the cell's active area and is automatically spread across the paths indicated when the cell is rotated to simulate off-normal incident light reception.

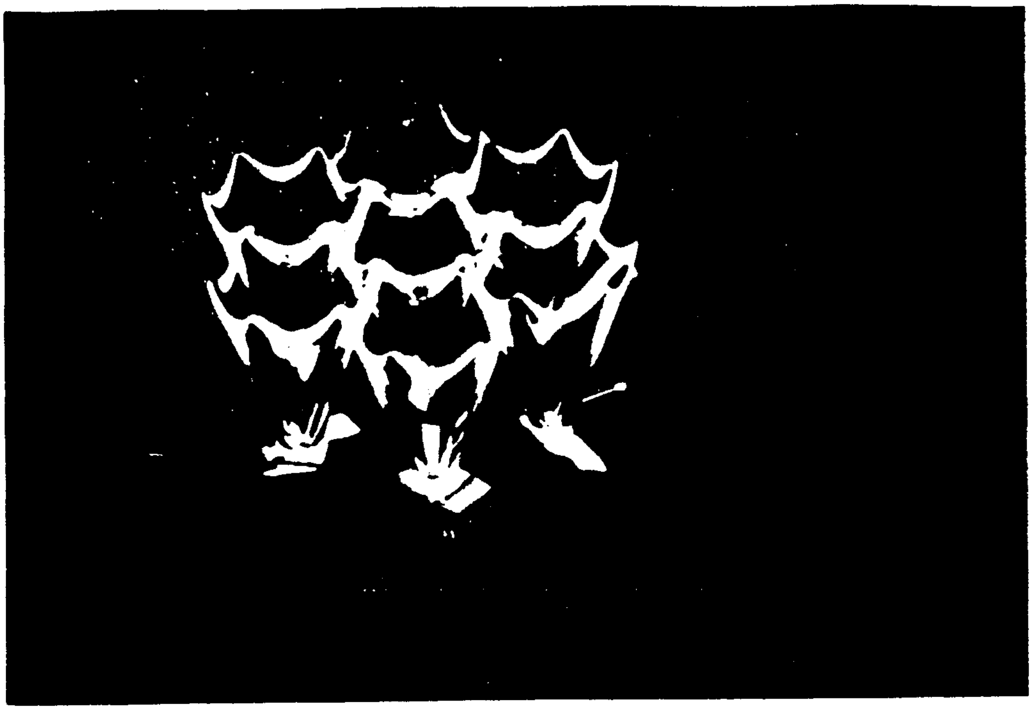

Figure 6-1. Structural Test Module

TEMP. = 26 Deg C

CELL AREA = .2 cm^2

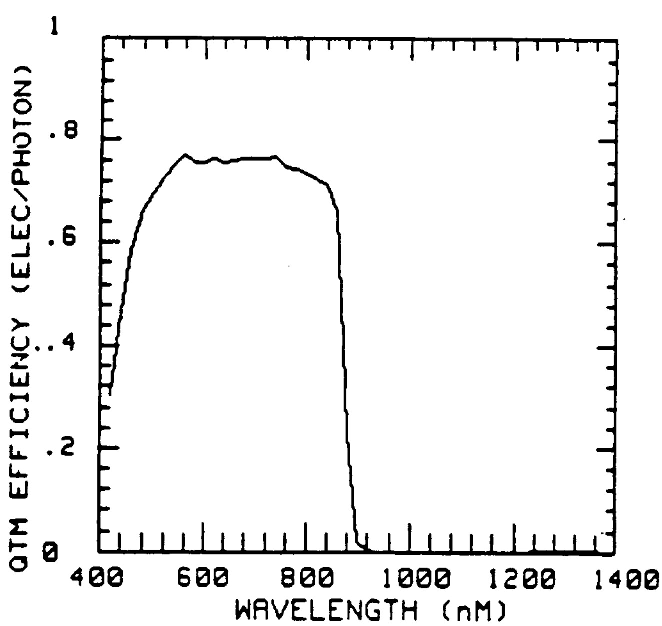

Figure 6-2. GaAs Concentrator Cell

Table 6-1. Sample: GaAs Concentrator Cell

SAMPLE: GaAs CONCENTRATOR CELL

TEMPERATURE = 26 Deg C
CELL AREA = .2 cm^2
REMARK: PRE RADIATION TEST

WAVELENGTH (nM)	CELL RESPONS. (Amp/W)	CELL QNTUM EFF. (ELECTRONS/PHOTON)	LIGHT INTENSITY (W/cm^2)	CELL CURRENT (AMP/cm^2)
420.0	1.0278E-01	3.0342E-01	1.4734E-05	1.5145E-06
440.0	1.6572E-01	4.6699E-01	8.6329E-05	1.4307E-05
460.0	2.1749E-01	5.8620E-01	1.1879E-04	2.5834E-05
480.0	2.5744E-01	6.6497E-01	1.4396E-04	3.7059E-05
500.0	2.7995E-01	6.9420E-01	1.7673E-04	4.9477E-05
520.0	3.0422E-01	7.2537E-01	2.0275E-04	6.1682E-05
540.0	3.2593E-01	7.4834E-01	2.2216E-04	7.2407E-05
560.0	3.4819E-01	7.7091E-01	2.3491E-04	8.1793E-05
580.0	3.5278E-01	7.5413E-01	2.4977E-04	8.8114E-05
600.0	3.6565E-01	7.5559E-01	2.5493E-04	9.3214E-05
620.0	3.8103E-01	7.6197E-01	2.5558E-04	9.7384E-05
640.0	3.8939E-01	7.5436E-01	2.5338E-04	9.8666E-05
660.0	4.0450E-01	7.5988E-01	2.4656E-04	9.9733E-05
680.0	4.1864E-01	7.6331E-01	2.4212E-04	1.0136E-04
700.0	4.2956E-01	7.6085E-01	1.9371E-04	8.3213E-05
720.0	4.4153E-01	7.6032E-01	2.3800E-04	1.0508E-04
740.0	4.5654E-01	7.6492E-01	2.7577E-04	1.2590E-04
760.0	4.5663E-01	7.4493E-01	3.0920E-04	1.4119E-04
780.0	4.6686E-01	7.4210E-01	3.2601E-04	1.5220E-04
800.0	4.7312E-01	7.3325E-01	2.9463E-04	1.3940E-04
820.0	4.7742E-01	7.2187E-01	3.3990E-04	1.6227E-04
840.0	4.8035E-01	7.0900E-01	3.7731E-04	1.8124E-04
860.0	4.5654E-01	6.5819E-01	4.4063E-04	2.0116E-04
880.0	1.6363E-01	2.3054E-01	5.1883E-04	8.4894E-05
900.0	1.2571E-02	1.7318E-02	5.7384E-04	7.2137E-06
920.0	1.0906E-03	1.4698E-03	6.1076E-04	6.6610E-07
940.0	3.3562E-04	4.4268E-04	6.6594E-04	2.2350E-07
960.0	8.5722E-05	1.1071E-04	7.4310E-04	6.3700E-08
980.0	7.3204E-05	9.2614E-05	8.0460E-04	5.8900E-08
1000.0	7.0924E-05	8.7935E-05	8.6290E-04	6.1200E-08
1020.0	7.4532E-05	9.0597E-05	8.8956E-04	6.6300E-08
1040.0	7.9183E-05	9.4399E-05	9.0929E-04	7.2000E-08
1060.0	8.1019E-05	9.4766E-05	9.0720E-04	7.3500E-08
1080.0	8.1620E-05	9.3702E-05	9.0541E-04	7.3900E-08
1100.0	8.7148E-05	9.8228E-05	8.9962E-04	7.8400E-08
1120.0	9.3055E-05	1.0301E-04	8.7260E-04	8.1200E-08
1140.0	9.8853E-05	1.0751E-04	8.5582E-04	8.4600E-08
1160.0	1.0245E-04	1.0950E-04	8.3750E-04	8.5800E-08
1180.0	1.1946E-04	1.2552E-04	8.1281E-04	9.7100E-08
1200.0	2.3327E-04	2.4102E-04	7.9264E-04	1.8490E-07
1220.0	5.1878E-04	5.2722E-04	7.6777E-04	3.9830E-07
1240.0	1.0418E-03	1.0417E-03	7.4536E-04	7.7650E-07
1260.0	1.6650E-03	1.6384E-03	7.2450E-04	1.2063E-06
1280.0	2.4451E-03	2.3685E-03	6.9632E-04	1.7026E-06
1300.0	3.2613E-03	3.1104E-03	6.6970E-04	2.1841E-06
1320.0	4.2598E-03	4.0012E-03	6.4446E-04	2.7453E-06
1340.0	5.0025E-03	4.6286E-03	6.1360E-04	3.0699E-06
1360.0	2.5408E-03	2.3164E-03	5.5541E-04	1.4112E-06
1380.0	5.8217E-04	5.2305E-04	5.3077E-04	3.0900E-07
1400.0	2.2756E-04	2.0153E-04	5.1020E-04	1.1610E-07

Table 6-1. Sample: GaAs Concentrator Cell (Continued)

```
THE TEST CELL CURRENT IS MEASURED BY FLUKE DVM

THE REFERENCE CELL CURRENT IS MEASURED BY HP DVM
MINIMUM WAVELENGTH= 420  (NM)
MAXIMUM WAVELENGTH= 1400  (NM)
WAVELENGTH INCREMENT= 20  NM

REFERENCE CELL IS Si CELL FOR WAVELENGTH<= 1000  nM

REFERENCE CELL IS Ge CELL FOR WAVELENGTH> 1000  nM
FOR LAMBDA < 700  nm GRATING IS 1180 GROOVE/mm
FOR LAMBDA >= 700  nm GRATING IS 590 GROOVE/mm
FOR LAMBDA < 800  nm SHORT waveleng filter is used
FOR LAMBDA >= 800  nm LONG waveleng filter is used

SCAN FROM LOW TO HIGH


I= 15  V_TEST(I-1)= .2079216  V_REF(I-1)= 1.07821006
VREF= .68505236  VTEST= .1288026 CR1= 1.0256409823
 TEST CELL CURRENT METER SCALE= 100
 REF. CELL CURRENT METER SCALE= 100
SLIT WIDTH = 2  MM

REFERENCE CELL IS Si CELL FOR WAVELENGTH < 1000   nM

REFERENCE CELL IS Ge CELL FOR WAVELENGTH >= 1000   nM
C_FACTOR=  1   RSP_SI= 0   RSP_GE= 0
```

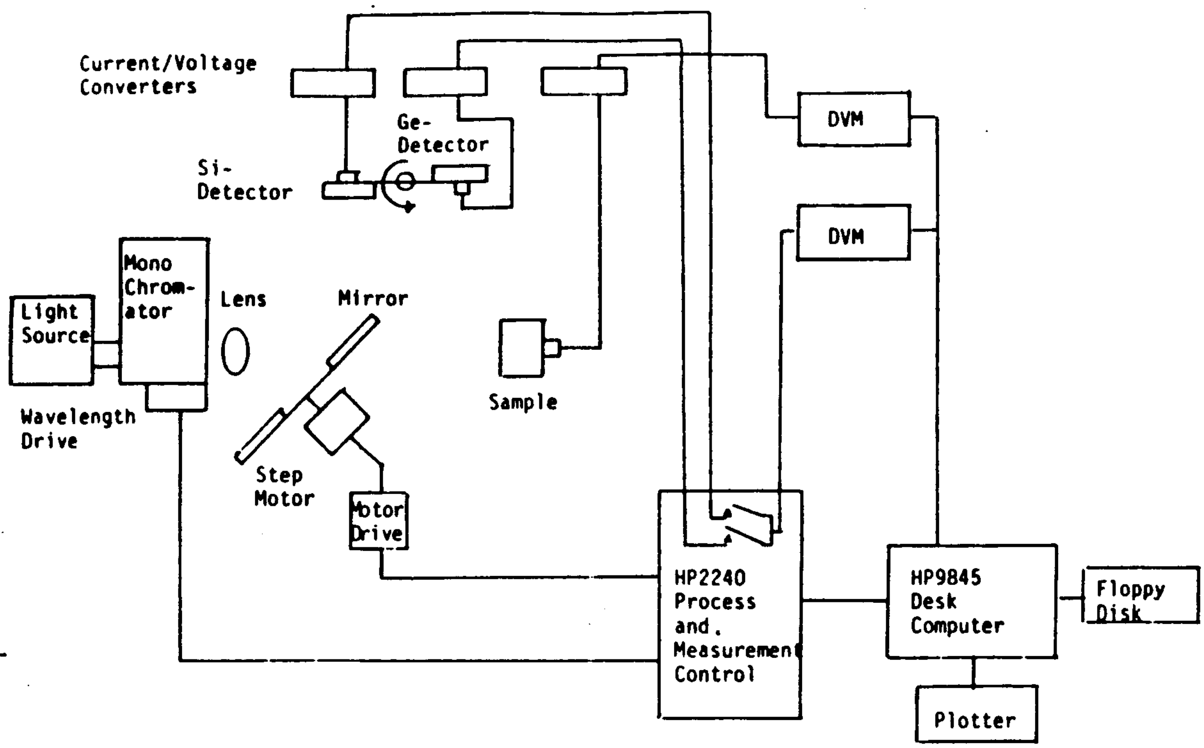

Figure 6-3. Schematic Diagram of Spectra Response Measurement System

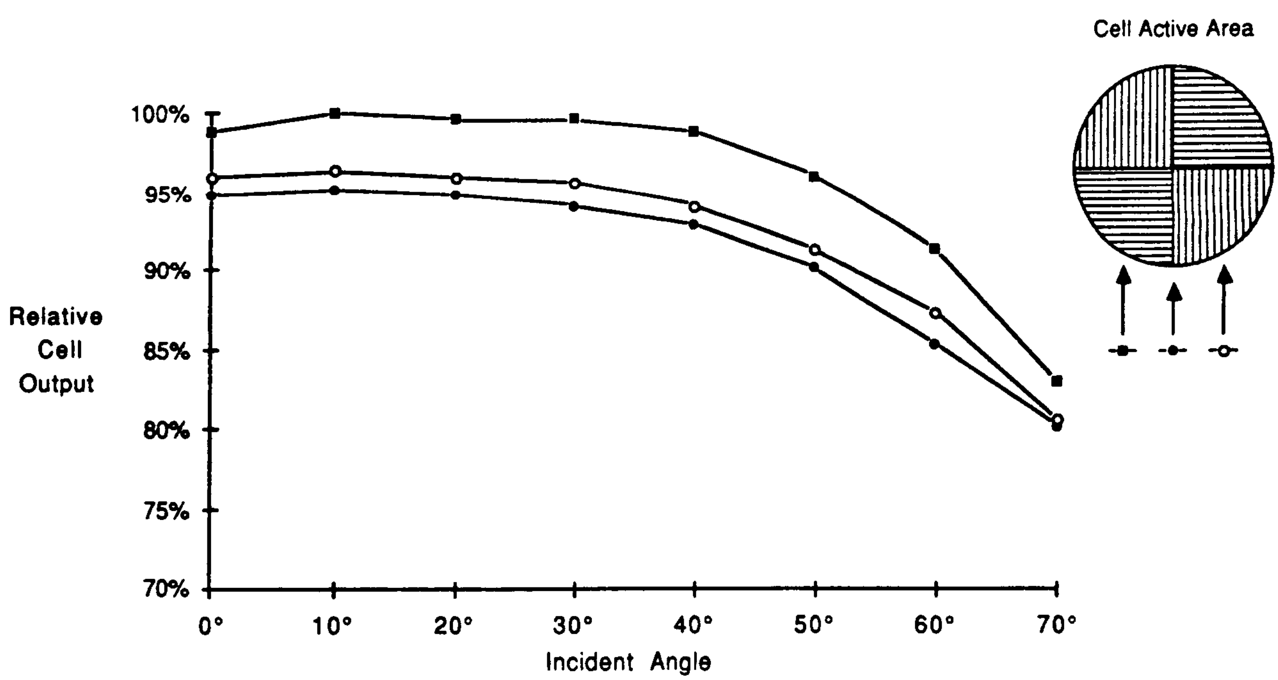

Figure 6-4. Cell Output Vs. Incident Angle

SECTION 7.0

THERMAL AND STRUCTURAL EVALUATION

Structural integrity was evaluated using the test module discussed in section 6. The module was mounted on a shake table and subjected to a typical launch vibration profile. No adverse effects were observed.

Thermal evaluation was determined using a single funnel and cell unit bonded in the same fashion as a unit from the above module. This unit was tested by thermal cycling as described in section 10. No damage resulted from this test.

SECTION 8.0

LABORATORY EVALUATION OF LIGHT FUNNELS

8.1 DIMENSIONAL DATA ON PROGRAM LIGHT FUNNELS

Boeing received a quantity of 12 light funnel elements from Weiss Scientific Glass Company. The funnels were fabricated from grade 7740 borosilicate glass. The funnel forming technique is proprietary to Weiss, but in general consists of expanding a glass tube with a graphite wedge while mounted in a glass lathe. Inside and outside walls are then ground to specifications. A solid plug of glass is fused to the small end of the cone and ground to match the outside wall. The end of the cone is then ground flat and the entire cone is lightly fire polished.

The dimensional parameters for the 12 light funnels manufactured by Weiss Scientific Glass and the light funnel design are presented in table 8-1. A graphical representation of cone angle variation is shown in figure 8-1. The outer cone angles could be directly calculated from dimensional data measured with a caliper; however, the inner angles could not be accurately measured due to uncertainty in the inner diameter of the cone upper edge. A bead formed at the cone lip as a result of the flame polishing finishing operation performed by Weiss Scientific Glass. The thickness of the beam varied from funnel to funnel, and in some funnels the lip sagged out of roundness. The base thickness dimension refers to the thickness of the solid glass base as measured from the apex of the inside wall of the cone to the flat face. The light funnels are exhibited varying degrees of roundness at the inner cone apex. These distortions from the light funnel design caused large variation in light funnel performance.

Due to the dimensional variations noted in table 8-1 it was necessary to rank the funnels with respect to performance and arrive at two similar groups to enable comparison of bare and AR-coated performance.

8.2 EXPERIMENTAL APPARATUS FOR LIGHT THROUGHPUT AND ANGULAR DEPENDENCE MEASUREMENTS

Since light exits the light funnels over a broad range of angles, an integrating sphere was used in conjunction with a collimated light source to evaluate the concentration factor and angular dependence of each funnel. These two properties were measured for both bare and AR-coated funnels. Figure 8-2 depicts the salient features of the apparatus used to measure light funnel throughput at normal and off-normal angles of incidence.

The light funnel mounting apparatus for the integrating sphere tests was designed to be adjustable, to accommodate the significant variation in the delivered light funnel physical dimensions. This adjustability was accomplished by having a fixed base aperture (0.175-in dia.) which is mounted flush to the integrating sphere inner surface, with a second annular support ring coaxial with the base aperture which can be translated along the common axis to accommodate the various outside cone angles. The inner surface of the mounting fixture was painted black to prevent fixture reflection from affecting light funnel performance data.

8.3 LIGHT FUNNEL EVALUATION USING INTEGRATING SPHERE APPARATUS

8.3.1 Uncoated Light Funnel Performance

The relative performance of the light funnels using the integrating sphere apparatus is presented in figure 8-3. The solid bars, identified as "not coated," illustrate the variation in light funnel performance due to dimensional nonuniformity. The concentration factor is determined by measuring the short circuit current response of a silicon detector mounted on the integrating sphere wall, with the light funnel base mounted flush to the sphere wall, versus measurements with the light funnel fixture removed. The detector current output is assumed to be proportional to the entering light intensity, and the light intenstiy ratio determining the concentration factor.

As illustrated in figure 8-3, light funnels #3 and #10 exhibited the highest concentration factors without coatings, with values of 11.9 and 11.5, respectively. Light funnels #6, #8 and #9 all exhibited similar performance with concentration ratios of approximately 10. These data led to the selection of these light funnels along with funnel #2 for use in antireflective coating experiments. The best performing light funnels (#3 and #10), had similar base diameter and wall angle dimensions, as indicated in table 8-1 and figure 8-1.

Near the end of this contract another light funnel became available which had been designed with a much lower concentration ratio and fabricated from fused silica (grade 7940). This funnel has been designated in the charts as "s1". The design concentration ratio for s1 was 12, and as can be seen from figure 8-3, the measured concentration of 8.8 is on the same order as the initial funnels. This result led to a decision to evaluate the efficiency of the funnels as shown in figure 8-4.. Funnel s1's efficiency of 78% was much higher than that of the higher concentration ratio funnels. The highest efficiency for the inital funnels was 38% after coating. There was no opportunity to coat funnel s1. The two different types of glass used (grade 7740 for the initial funnels and grade 7940 for funnel s1) were tested for transmittance. The results are shown in figure 8-5. A thickness of 3 cm was chosen for testing because modeling indicated this as the average pathlength for light throught the funnels. The borosilicate glass (7740) showed a marked absorption, particularly in the longer wavelengths as compared to the fused silica (7940). The drawing for funnel s1 is shown in figure 8-6, the only exception being that the tested funnel did not have the six facets shown in the figure.

8.3.2 Light Funnel Pointing Angle Tolerance

Angular dependence on light funnel throughput was measured for 10 funnels using the integrating sphere apparatus. The test procedure was to initially position the funnel and sphere platform to obtain a sphere-detector output maximum. Readings were then taken over a range of angles on either side of the maximum. An additional set of readings was taken at 90 degrees to the first set to evaluate funnel symmetry.

Plots of light funnel performance versus pointing angle with respect to the incident light, independent of solar cell performance were shown in figures 8-7 through 8-17. These data indicate that within a pointing angle tolerance of ± 2 degrees the light funnel performance is approximately 94% of maximum, and within ± 1 degree of the performance is approximately 98% of maximum. This relatively wide pointing angle tolerance is very desirable when considering the assembly and alignment of large arrays of light funnel concentrators. Figure 3-2 presents the theoretical pointing angle tolerance of light funnel designs when the internal cone angle is held constant at 20 degrees and the external cone angle is varied. When the actual pointing angle data is compared to the theoretical model, the wider angle tolerance in the measured performance indicates the actual cone angle difference in the delivered cones is greater than the design specified. This variation from the light funnel design contributed to the lower concentration factors of the actual light funnel than was predicted in the design phase.

8.3.3 Light Funnel Base AR-Coating Results

An antireflective coating of MgF_2 was applied to the bases of light funnels #2, #6, #9 and #10 by a vendor outside of Boeing. The requested coating was 1.05 KA (1 QWOT at γ = 550 nm 18 deg angle in glass). The vendor optically estimated the film thickness on witness slides, which were later measured to be approximately 0.75 KA thick. This results in the AR-coating being less effective than optimum.

Light funnel #9 had the AR-coating applied to the base surface only. The data illustrated in figure 8-3 shows a 27% increase in concentration ratio with the base AR-coated in comparison to the uncoated result. This significant improvement in performance indicates much of the light trapped in the light funnel impinges on the base plane at incident angles close to the critical angle, which results in large reflection ratios. The AR-coating was the most significant effect on the light funnel performance when large amounts of reflection occurs at the coated surface.

Any light incident or incident on the base plane at angle greater than the critical angle (θ_C = 41.9 deg) is subject to total internal reflection, and does not exit the base plane, regardless of any coatings applied between the glass and air.

Variations in light funnel dimensions alter the distribution of the trapped light angles of incidence with the funnel base plane. Thus, the base AR-coating affects the light funnel performance differently for the various funnels.

8.3.4 Inner Cone AR-Coating Results

A MgF_2 antireflective coating was applied to the inner cone surface of light funnels #2, #3, #6 and #10 by the outside vendor who applied the base coating. The actual coating thickness on the light funnels is uncertain due to the geometrical differences in the mounting of the light funnels and the witness slide used in visually monitoring the coating thickness.

Light funnel #3 had an AR-coating applied only to the inner cone surface. As illustrated in figure 8-3, this funnel exhibited a 26% increase in concentration ratio when comparing the AR-coated to the uncoated performance data. The expected performance improvement theoretically is approximately 5% when considering only reflection reduction at a 70 degrees inclined surface. A secondary effect of the AR-coating is a microscopic smoothing of the coated surface. Surface tension binds the coated material more energetically in pits and valleys than on high points. This effect decreases the scatter in light reflecting in the light funnel, improving the light throughput. Another effect of the AR-coating is translation of the reflection locations down the light funnel. As a light ray intersects the AR-coated interface from the higher index bulk glass, the ray is refracted further away from normal, causing a translation in the point of reflections down the cone surface. This effect would reduce the total number of reflections the light undergoes, and subsequently reduces the number of rays with high angles of incidence with the base plane. This would reduce the reflection from the base surface.

8.3.5 Experimental Control

Light funnel #8 was reserved as a control constant in the coating experiments, with no AR-coatings applied. The light funnel concentration ratio was approximately 9% higher when measured along with the AR-coated funnels in comparison to the initial uncoated test data. This difference was probably due to poor seating in the light funnel mounting fixture in the uncoated funnel test. When light funnel #8 is well seated in the mounting fixture, the base is just flush with the integrating sphere inner surface. In the first test of the uncoated light funnels, the mounting fixture was freshly painted, and any protrusion in the mounting fixture cone would translate the light funnel base away from the integrating sphere surface. The light exiting the funnel base at extremely off-normal angles would be absorbed in the mounting fixture, rather than entering the integrating sphere cavity.

In the later light funnel tests, the funnels were adjusted in the mounting fixture until the best seating was achieved. This phenomenon would have little affect on the light funnels with smaller base diameter (#2, #3, #6, #10 and #12) since the base of these funnels protruded slightly into the sphere when mounted in the fixture.

Table 8-1. Dimensions of 12 Borosilicate Light Funnels

	O.D. TOP		O.D. BOTTOM		OVERALL HEIGHT		BASE THICKNESS
	MIN	MAX	MIN	MAX	MIN	MAX	
1	0.954	0.966	0.171	0.172	1.286	1.290	0.0950
2	0.942	0.950	0.153	0.156	1.275	1.278	0.0845
3	0.956	0.972	0.150	0.153	1.321	13126	0.1320
4	0.965	0.950	0.170	0.173	1.276	1.302	0.1040
5	0.977	0.986	0.172	0.173	1.281	1.291	0.0465
6	0.952	0.963	0.158	0.162	1.328	1.326	0.1520
7	0.973	0.983	0.179	0.180	1.296	1.299	0.0600
8	0.9785	0.990	0.165	0.168	1.305	1.310	0.0680
9	0.981	0.985	0.176	0.177	1.342	1.345	0.1040
10	0.977	0.980	0.152	0.155	1.366	1.369	0.1410
11	0.976	0.978	0.173	0.175	1.265	1.266	0.0410
12	0.971	0.979	0.155	0.157	1.313	1.317	0.0880
Design	0.945"		0.158"		1.323"		0.0827"

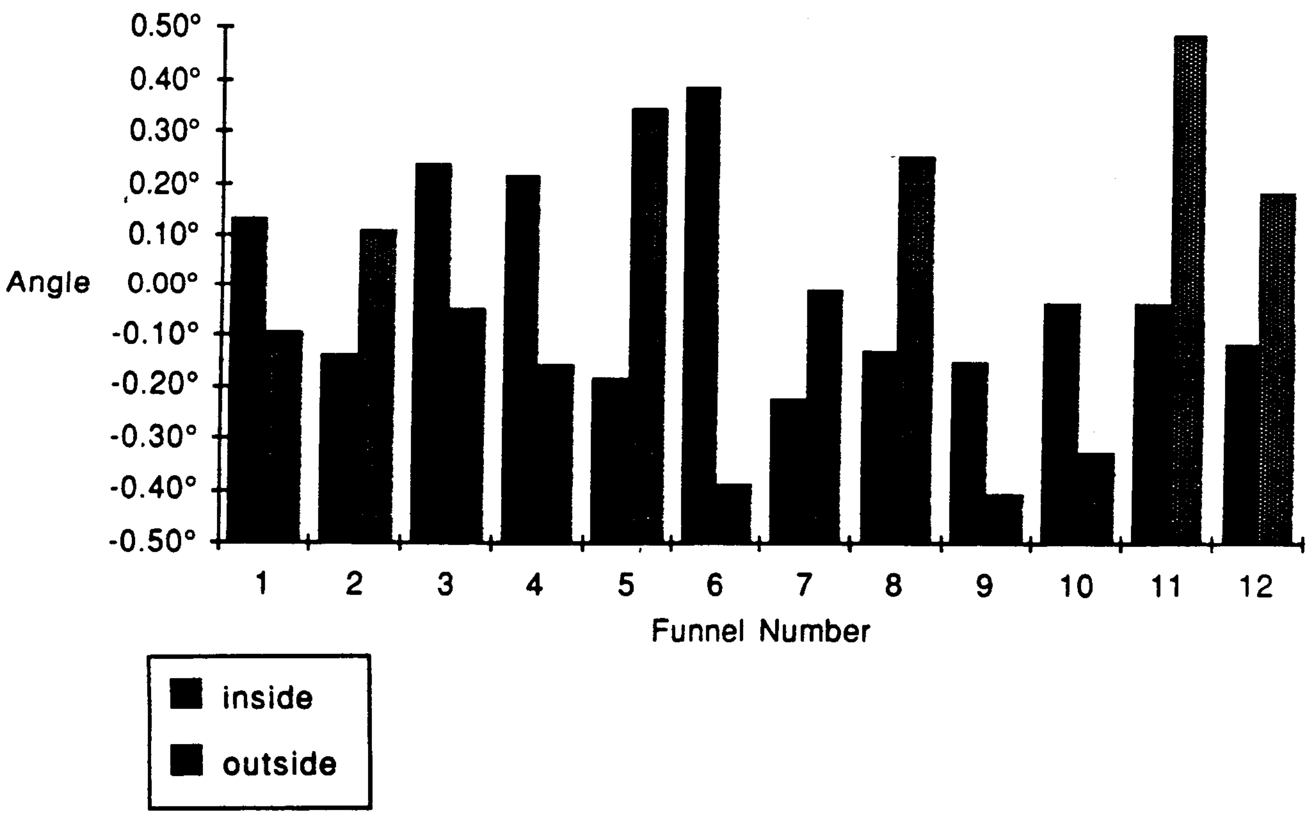

Figure 8-1. Funnel Angle Deviations From Mean

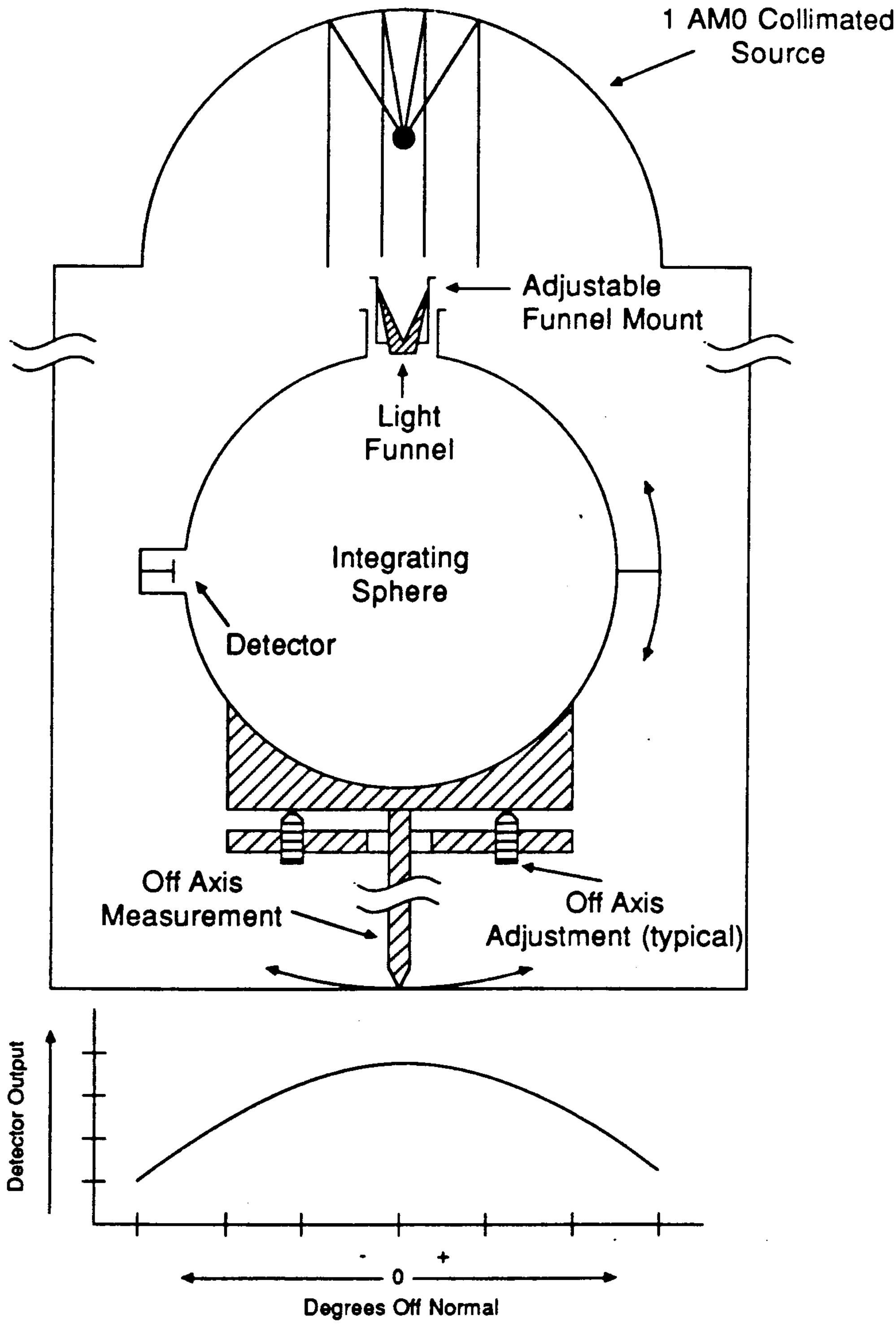

Figure 8-2. Light Funnel Throughput and Angular Dependance Schematic

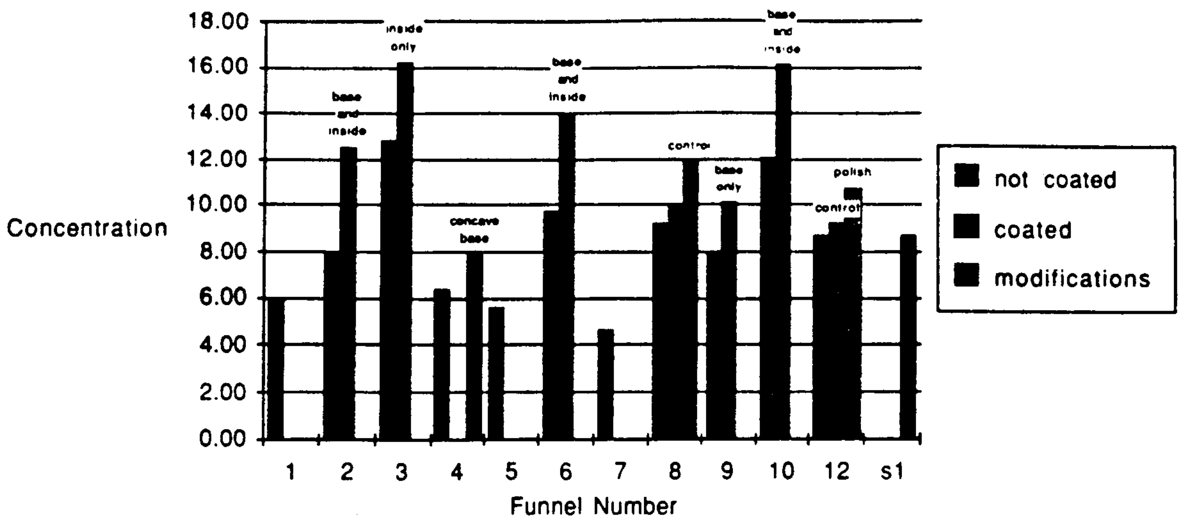

Figure 8-3. Light Funnel Concentration Into Integrated Sphere

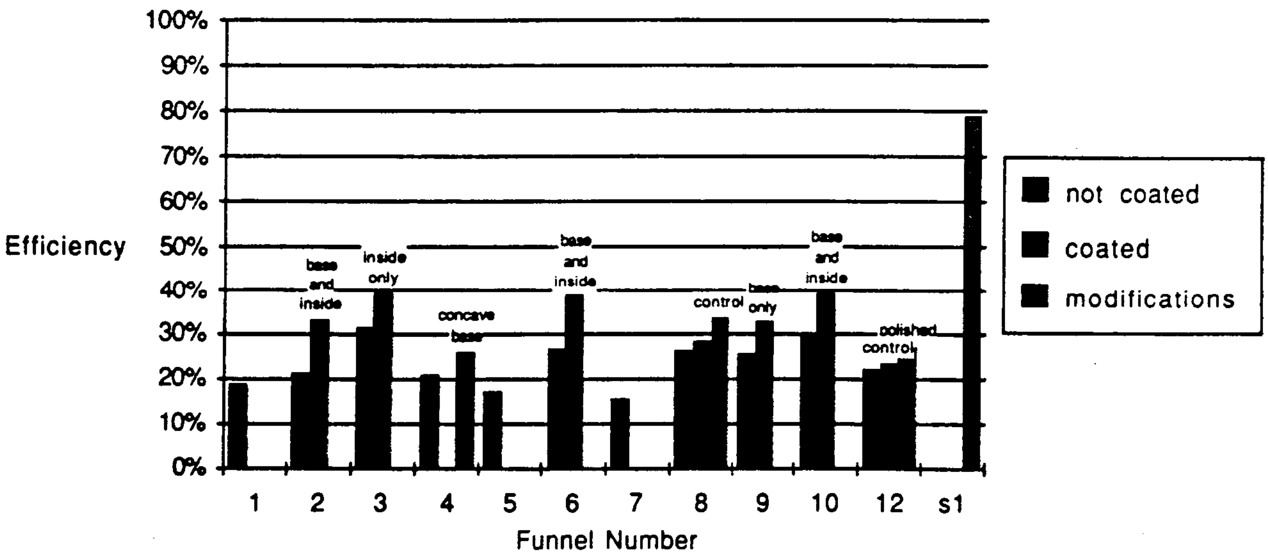

Figure 8-4. Light Funnel Efficiency Into Integrating Sphere

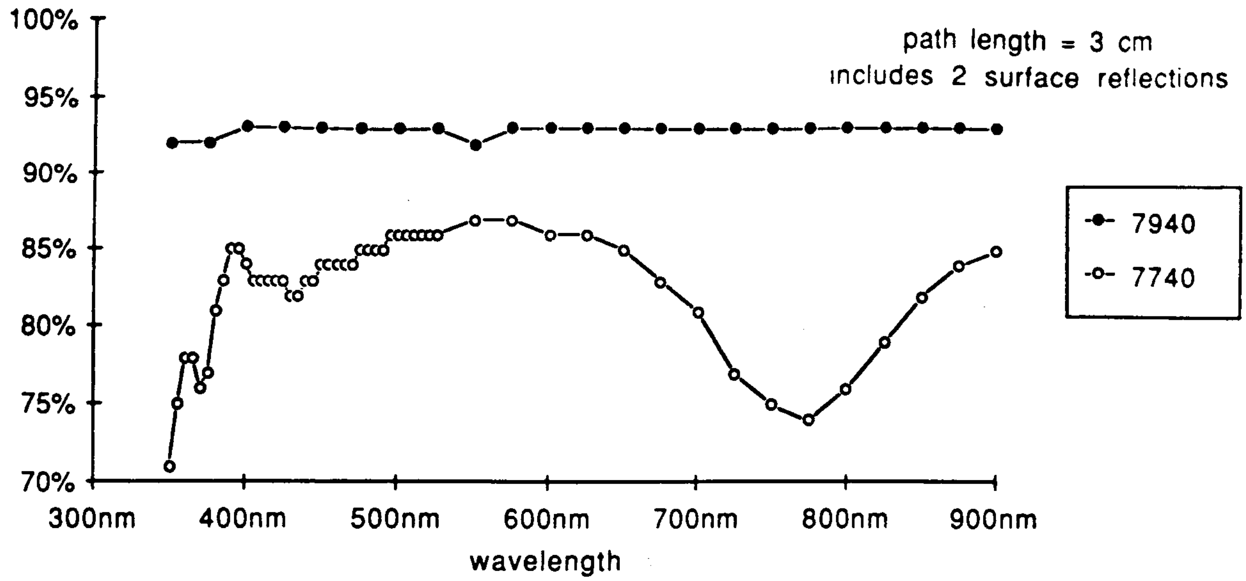

Figure 8-5. Spectral Transmittance

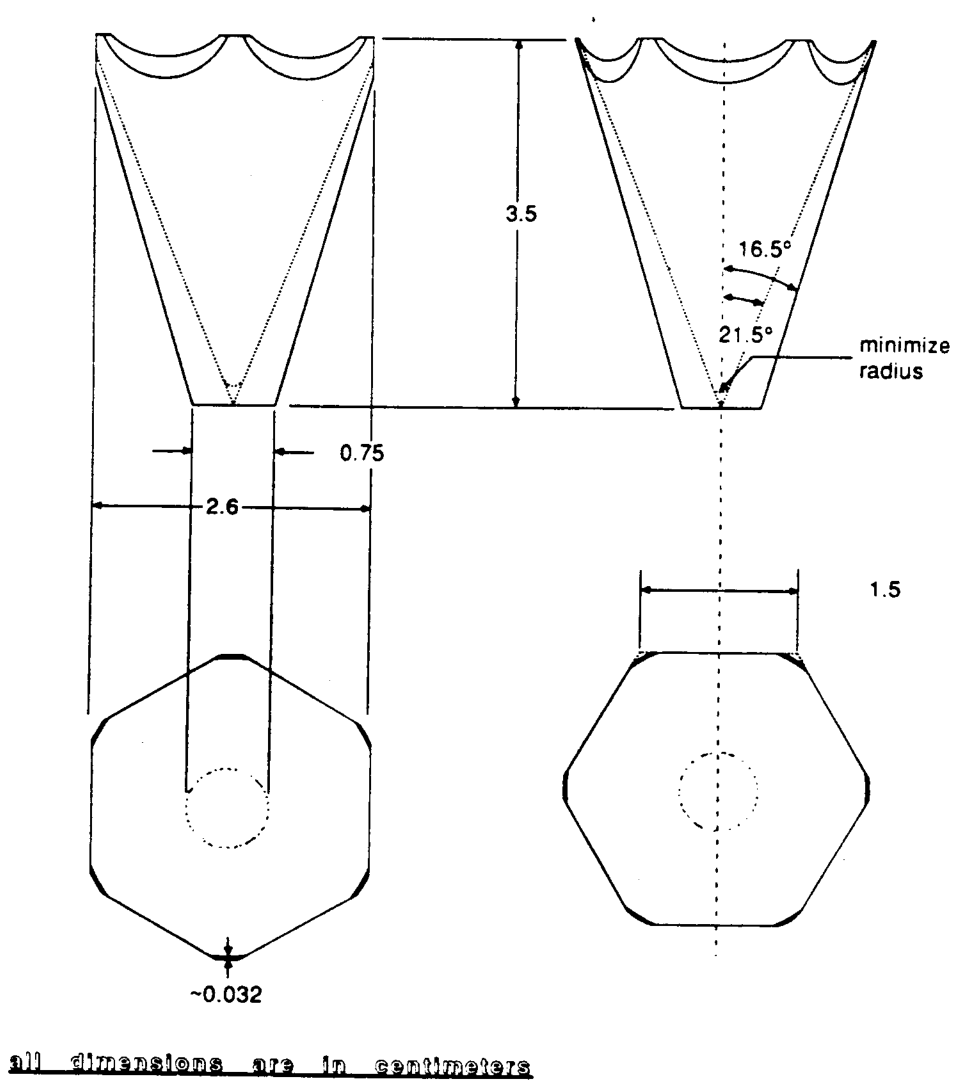

Figure 8-6. Modified Light Funnel

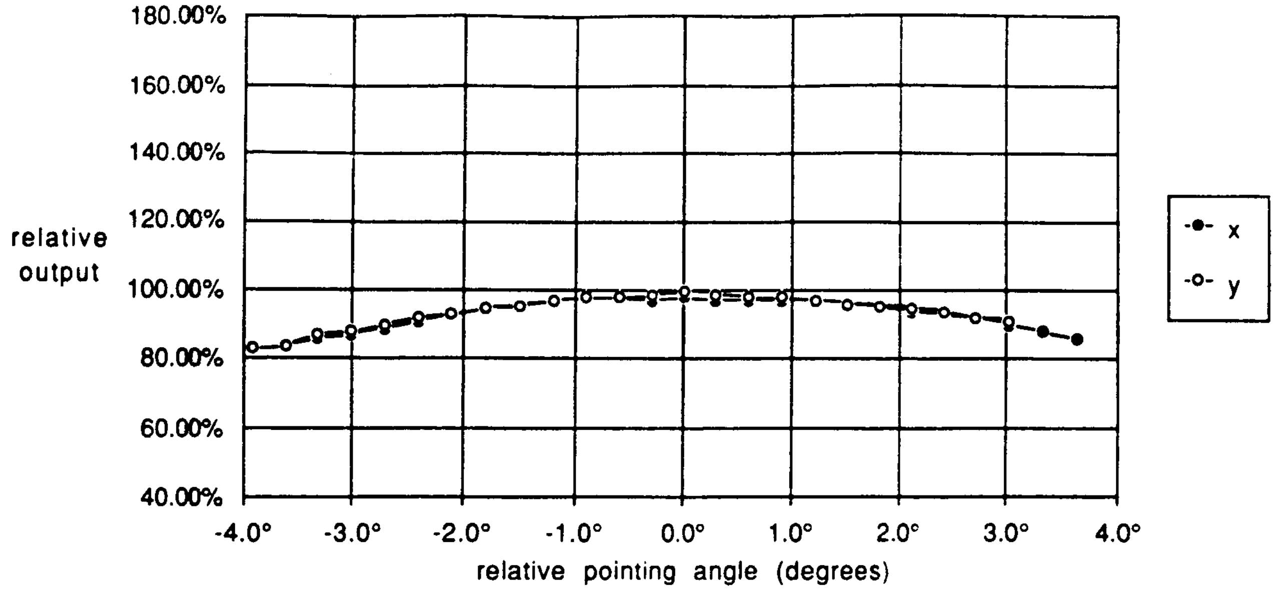

Figure 8-7. Light Funnel 1

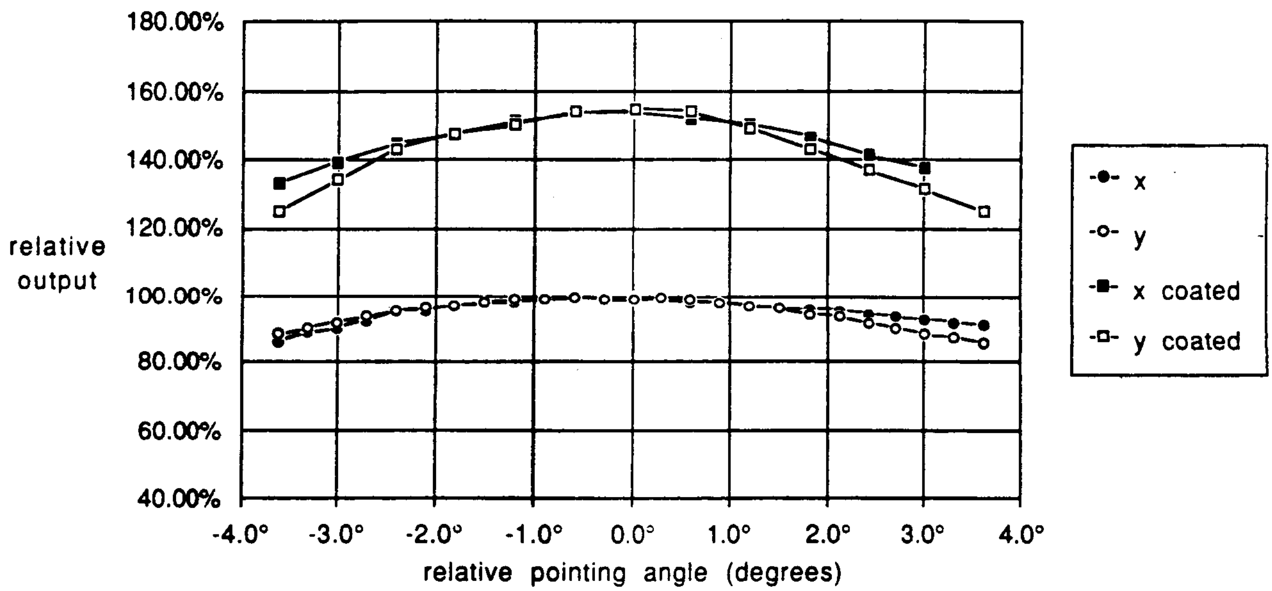

Figure 8-8. Light Funnel 2

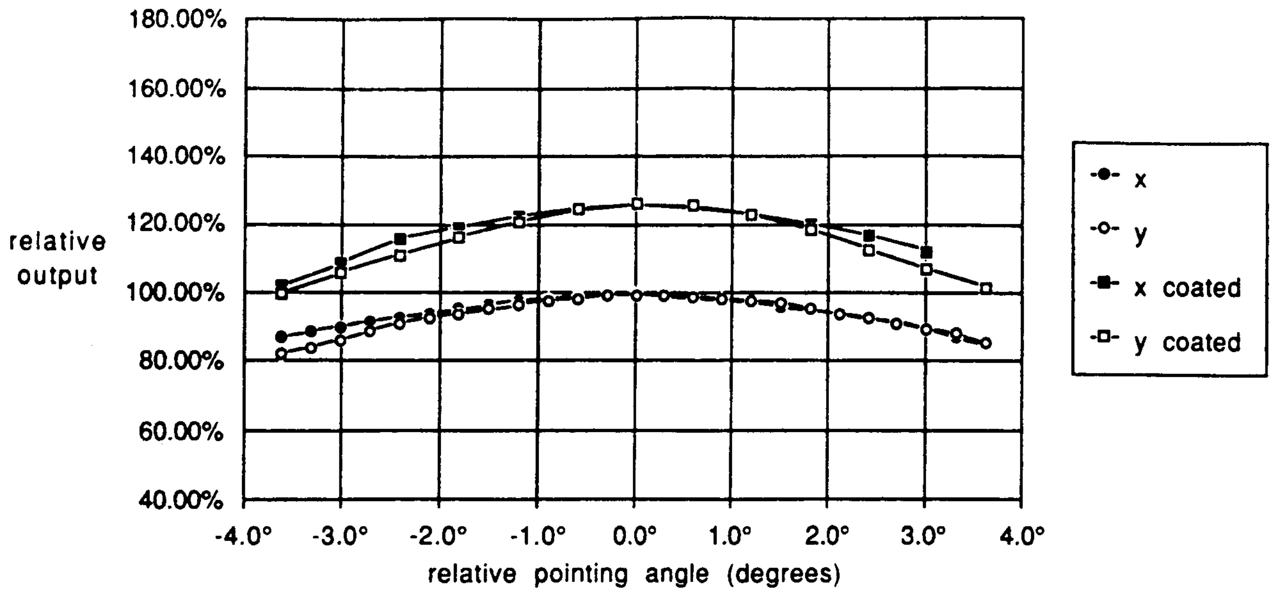

Figure 8-9. Light Funnel 3

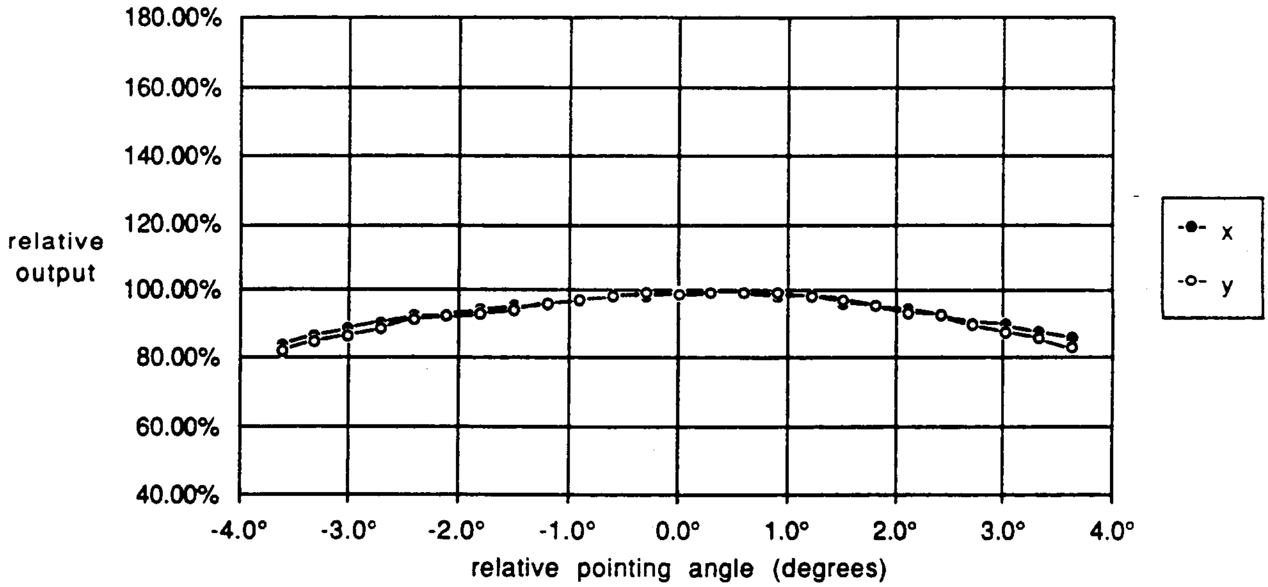

Figure 8-10. Light Funnel 4

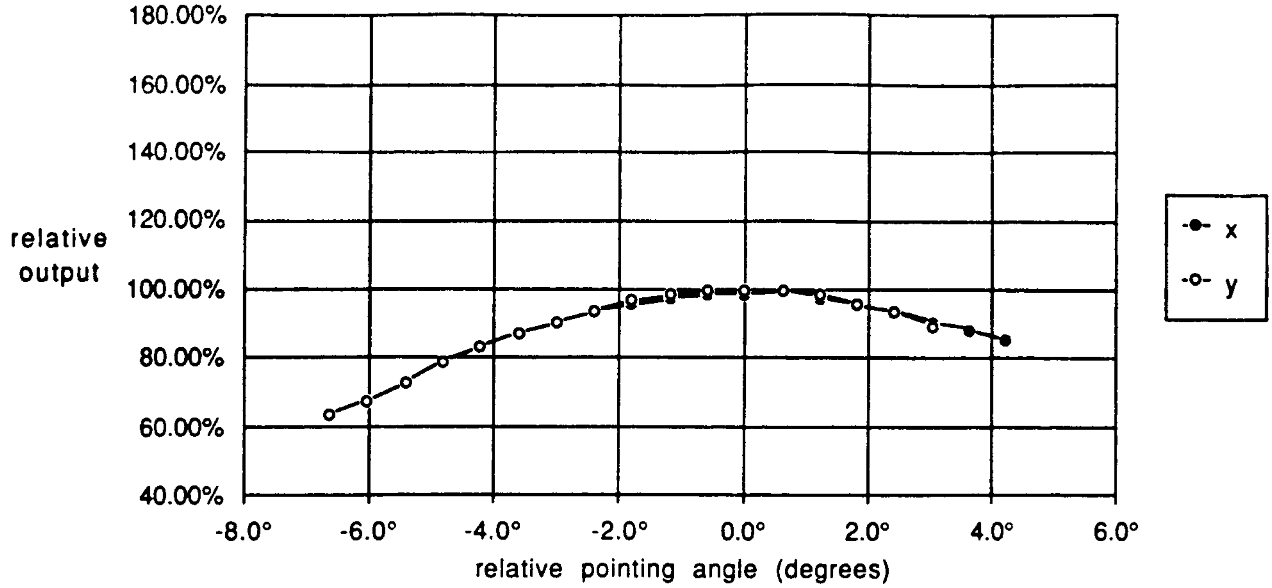

Figure 8-11. Light Funnel 5

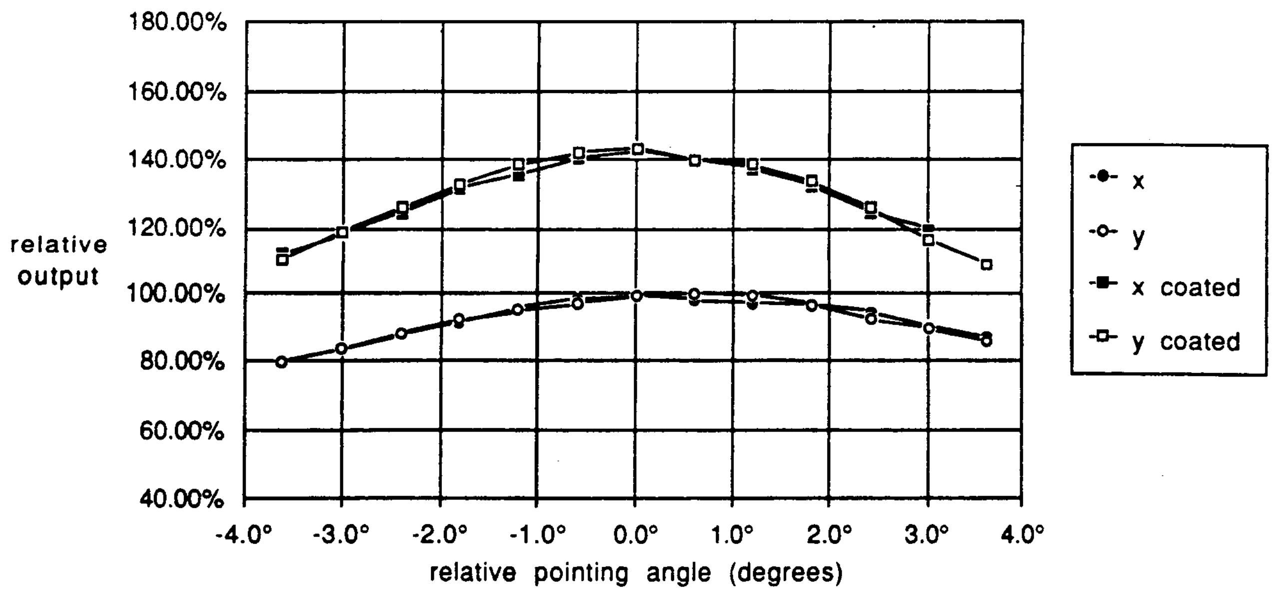

Figure 8-12. Light Funnel 6

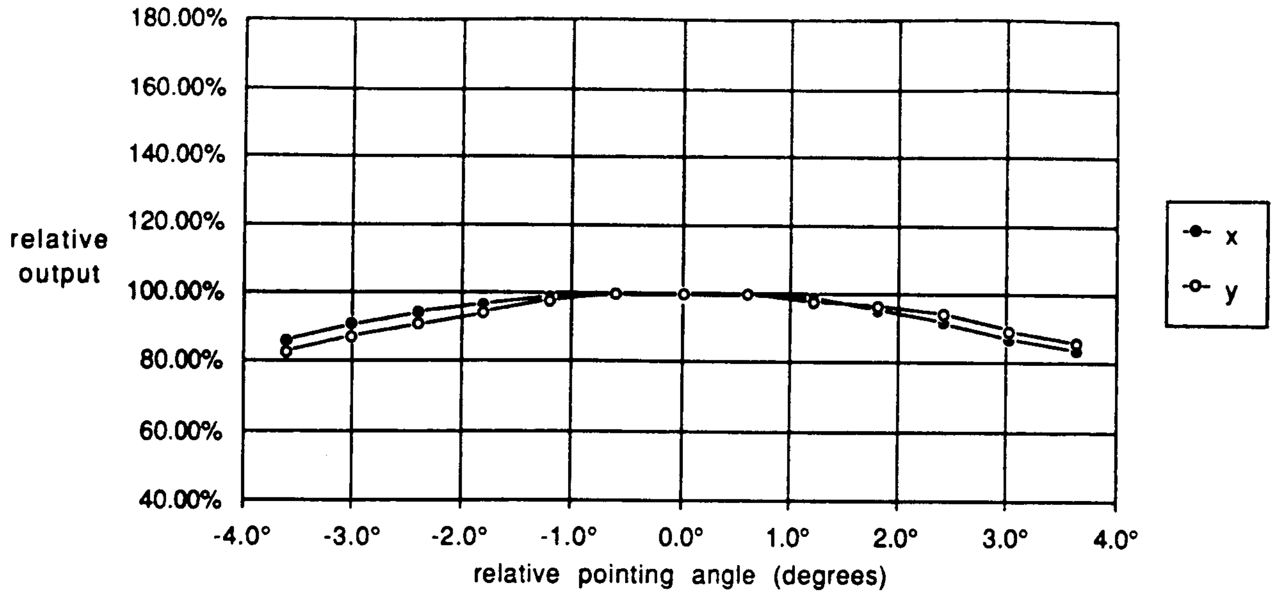

Figure 8-13. Light Funnel 7

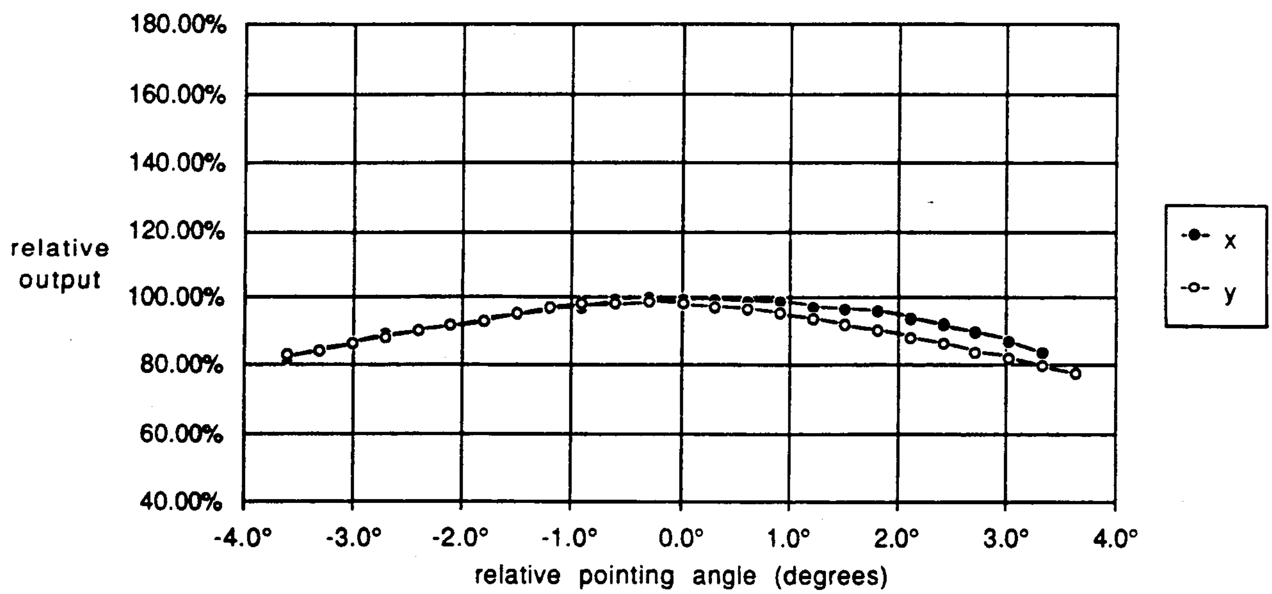

Figure 8-14. Light Funnel 8

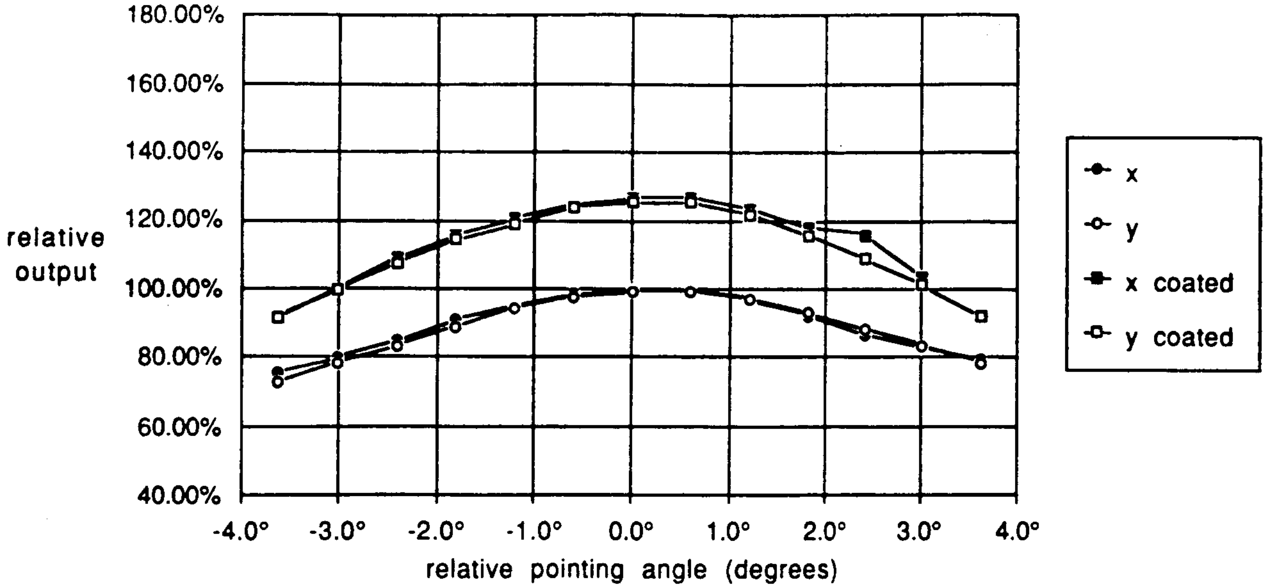

Figure 8-15. Light Funnel 9

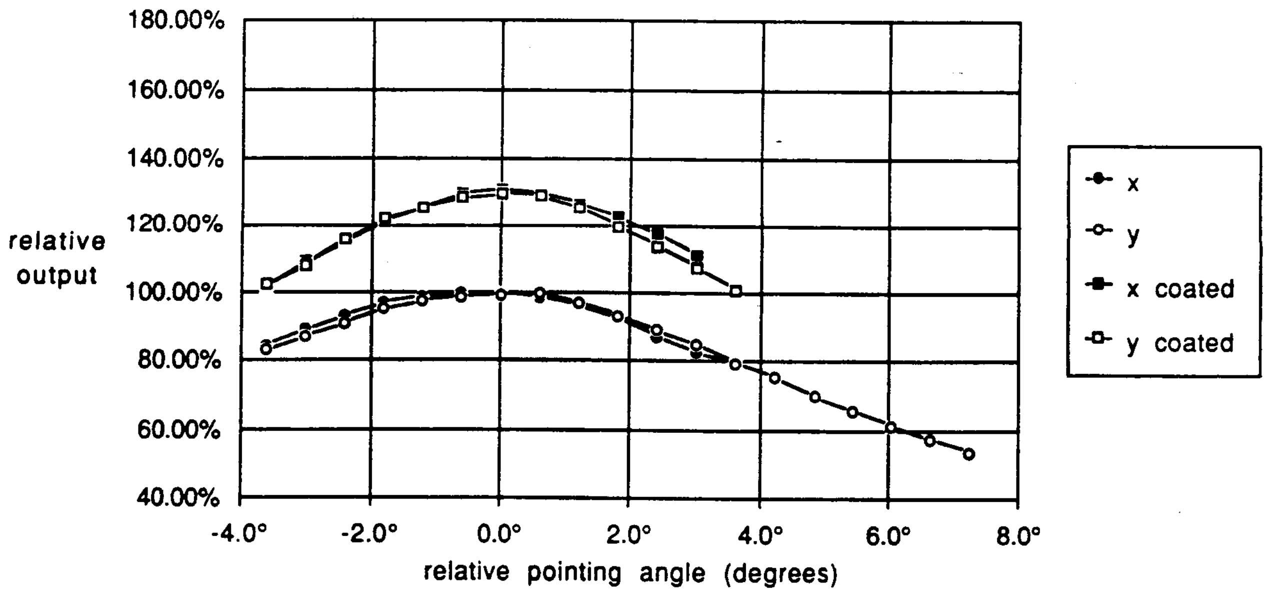

Figure 8-16. Light Funnel 10

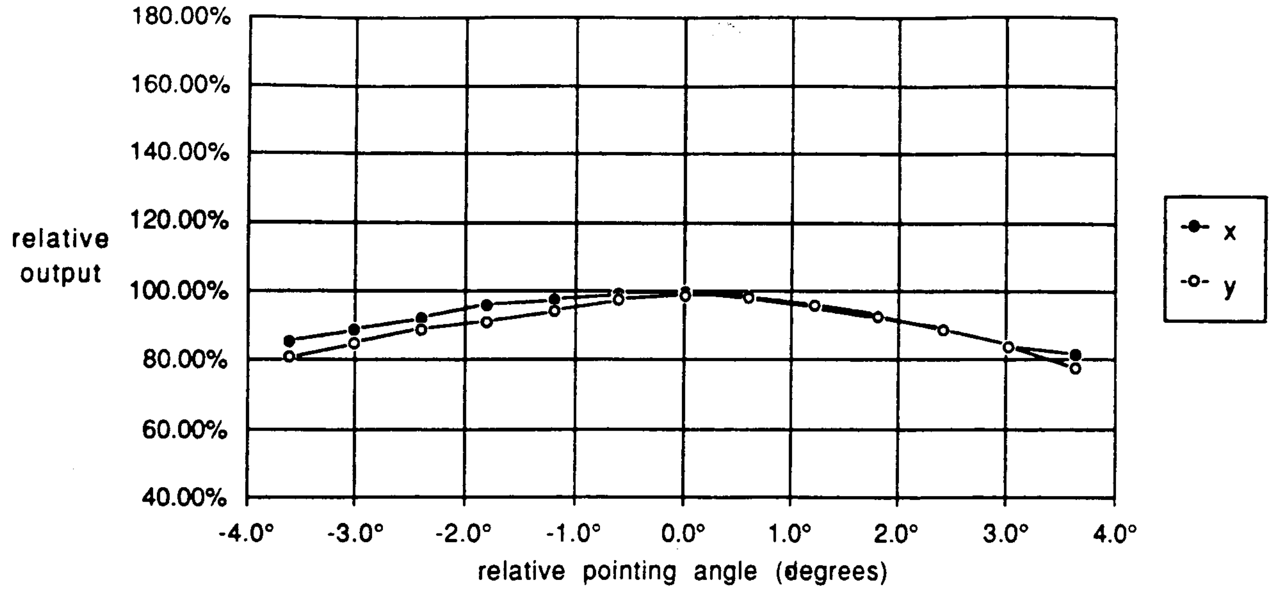

Figure 8-17. Light Funnel 12

SECTION 9.0

LABORATORY EVALUATION OF FUNNEL AND CELL ASSEMBLY

9.1 EXPERIMENTAL DESIGN

Angular dependence on cell output for the light funnel and cell assembly configuration was measured by replacing the integrating sphere with this assembly in the previously described apparatus.

The light funnel and cell assembly consisted of a GaAs solar concentrator cell mounted onto a test platform which accommodated spring-loaded mounting clips to hold individual light funnels in good contact with the cell. DC-93500, without the hardener, provided optical coupling between the funnel and cell. Comparative data could thus be obtained using the same cell. The test platform was water-cooled to eliminate thermal effects.

9.2 LIGHT FUNNEL AND CELL ASSEMBLY PERFORMANCE

The concentration ratio performance of various light funnels mounted to a Kopin GaAs concentrator cell is presented in figure 9-1. Initial uncoated data was taken only for light funnels #9 and #10. They were chosen as being representative of two groups of light funnels which exhibited similar performance in the uncoated integrating sphere test. The original intent was to coat only these two light funnels with AR-coatings, but further negotiations with the coating vendor resulted in AR-coating a group of four funnels on the inside cone, and coating four funnels in a separate run on the base surface. The light funnel #9 data indicates the base coating had little effect on the light funnel and cell assembly performance as expected, due to the close matching index of refraction of the MgF_2 AR-coating ($n = 1.38$) and the DC-93500 cell to funnel bonding adhesive ($n = 1.41$). Light funnel #10 demonstrated approximately 15% improvement in concentration performance due primarily to the inside AR-coating. The performance improvement of funnel #10 due to the AR-coating measured in the integrating sphere tests was approximately 30% (fig. 8-3). This suggests roughly half of the performance improvement comes from inner cone AR-coating and half from the base AR-coating in the integrating sphere tests. The spread in light funnel concentration performance is less for the various light funnels when measured bonded to the solar cell. This is further evidence that the distribution of light incident on the base at near the critical angle was a key cause of the wide range of light funnel performance measured in the integrating sphere test. When the funnels are optically coupled to a solar cell, the light is diffracted toward the normal, and does not undergo total internal reflection. Thus, most of the light incident on the base plane is transmitted to the solar cell.

Plots of solar cell electrical output versus light funnel and cell assembly pointing angles are presented in figures 9-2 and 9-3 for light funnels #9 and #10. These plots are very similar to the results plotted in figures 8-12 and 8-13, indicating the light funnel response is dominant in determining the pointing angle tolerance of a light funnel module. Again we see only about 2% decrease in module performance with an off-angle orientation of ± 1 degree, and approximately a 6% drop for an off-angle orientation of ± 2 degrees.

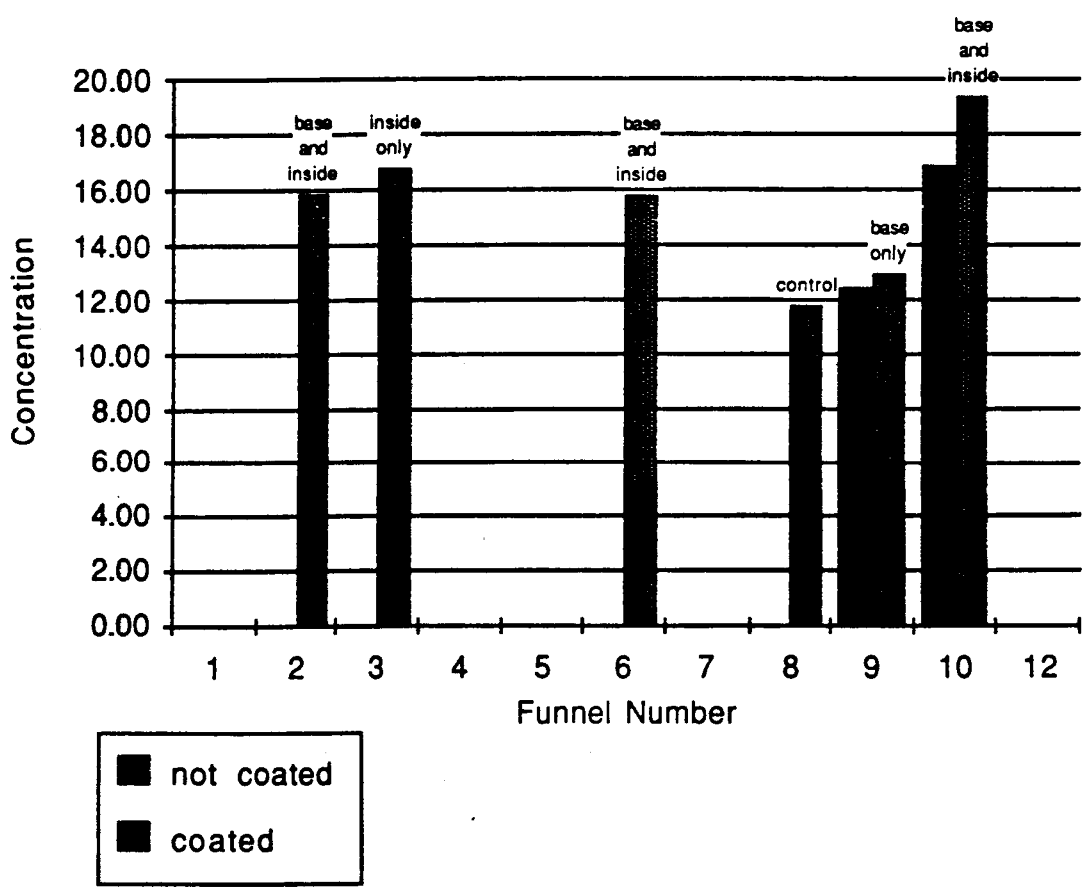

Figure 9-1. Light Funnel Concentration onto GaAs Concentrator Cell

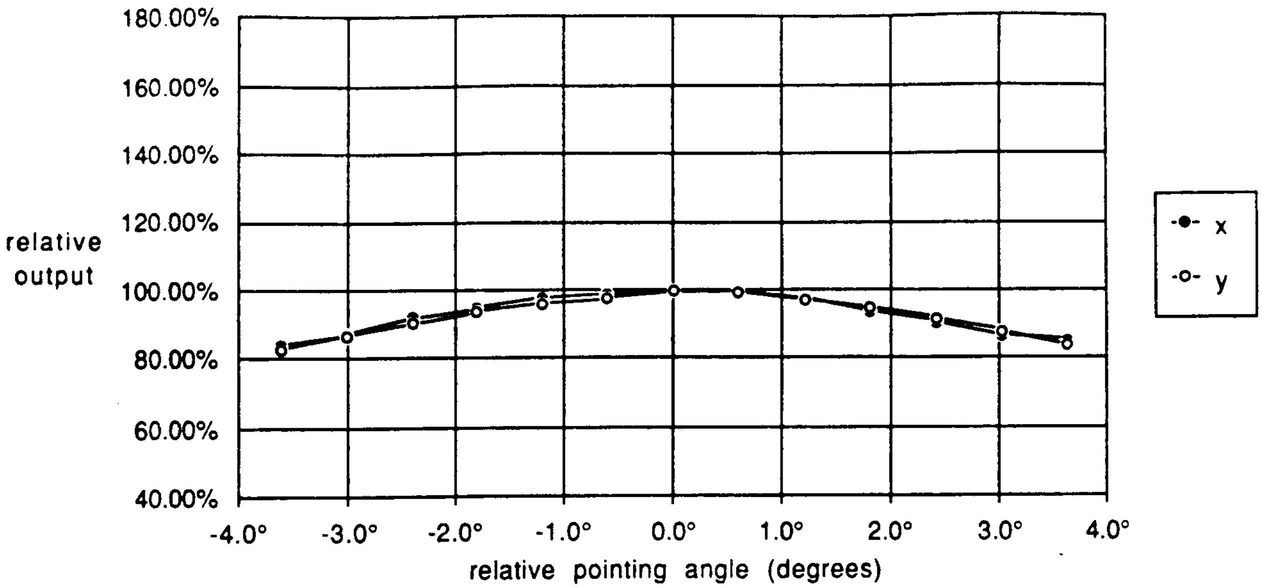

Figure 9-2. Light Funnel 9 on GaAs Cell

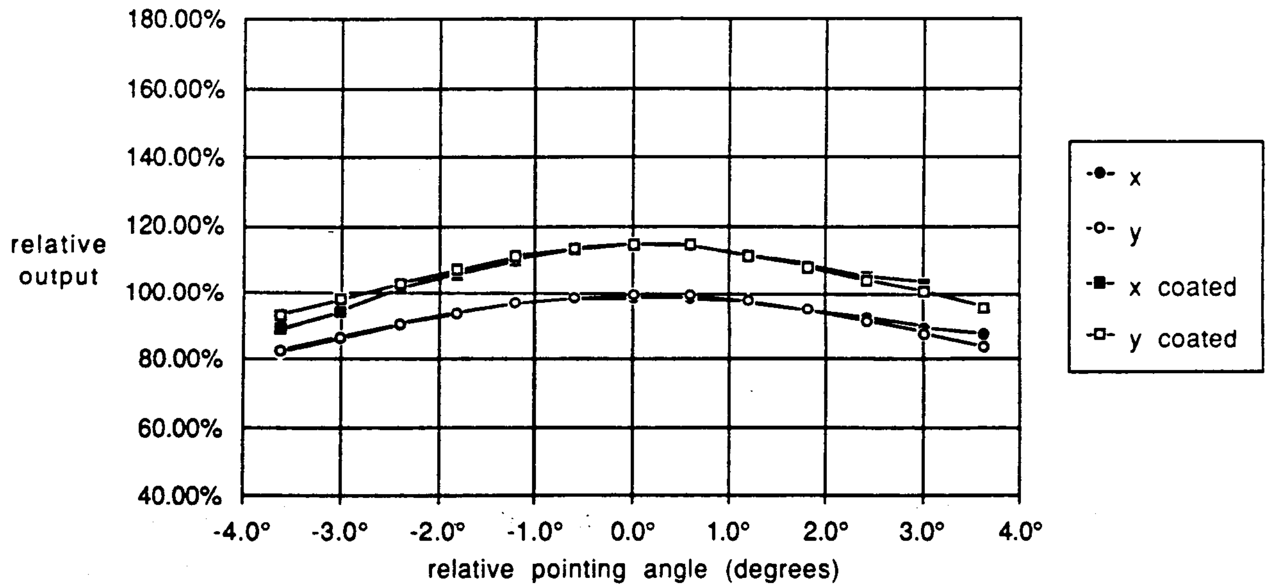

Figure 9-3. Light Funnel 10 on GaAs Cell

SECTION 10.0

THERMAL CYCLING OF FUNNEL AND CELL ASSEMBLY

Figure 10-1 depicts the test article used in the thermal cycle test. It consists of a light funnel bonded with DC-93500 to a GaAs concentrator cell which is soldered to a copper-plated slide glass. A thermocouple is welded to the cell. The slide glass is clip mounted to an arm inside a vacuum chamber. The chamber houses a radiant heat lamp and a LN_2 cold wall. The arm alternates between the lamp and cold wall to accomplish thermal cycling.

10.1 THERMAL CYCLE DATA

A total of 30 cycles revealed no change in cell output and no structural or visible damage was observed. A typical cycle was from +66°C to -30°C requiring 20 minutes to reach the upper temperature and 40 minutes to reach the lower temperature.

The upper temperature of +66°C was easily achieved using the in-situ radiant lamp but the lower temperature was restricted to -30°C due to a limited view factor of the test assembly to the cold wall. Figure 10-2 shows the funnel and cell assembly in the thermal cycle test chamber during the heating phase of a cycle. A vacuum of 10^{-6} torr was maintained throughout cycling.

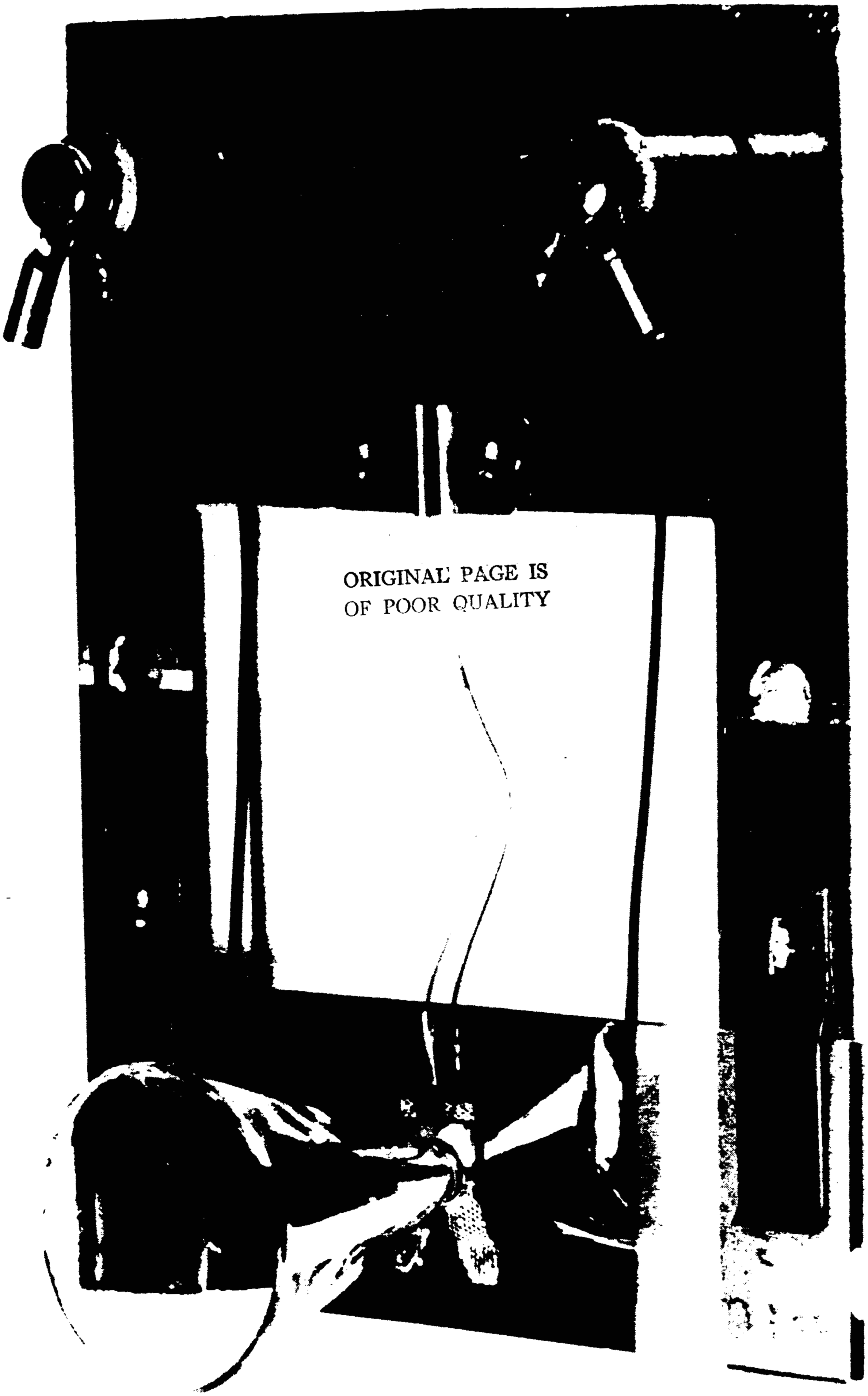

Figure 10-1. Assembly of GaAs Concentrator Cell and Light Funnel

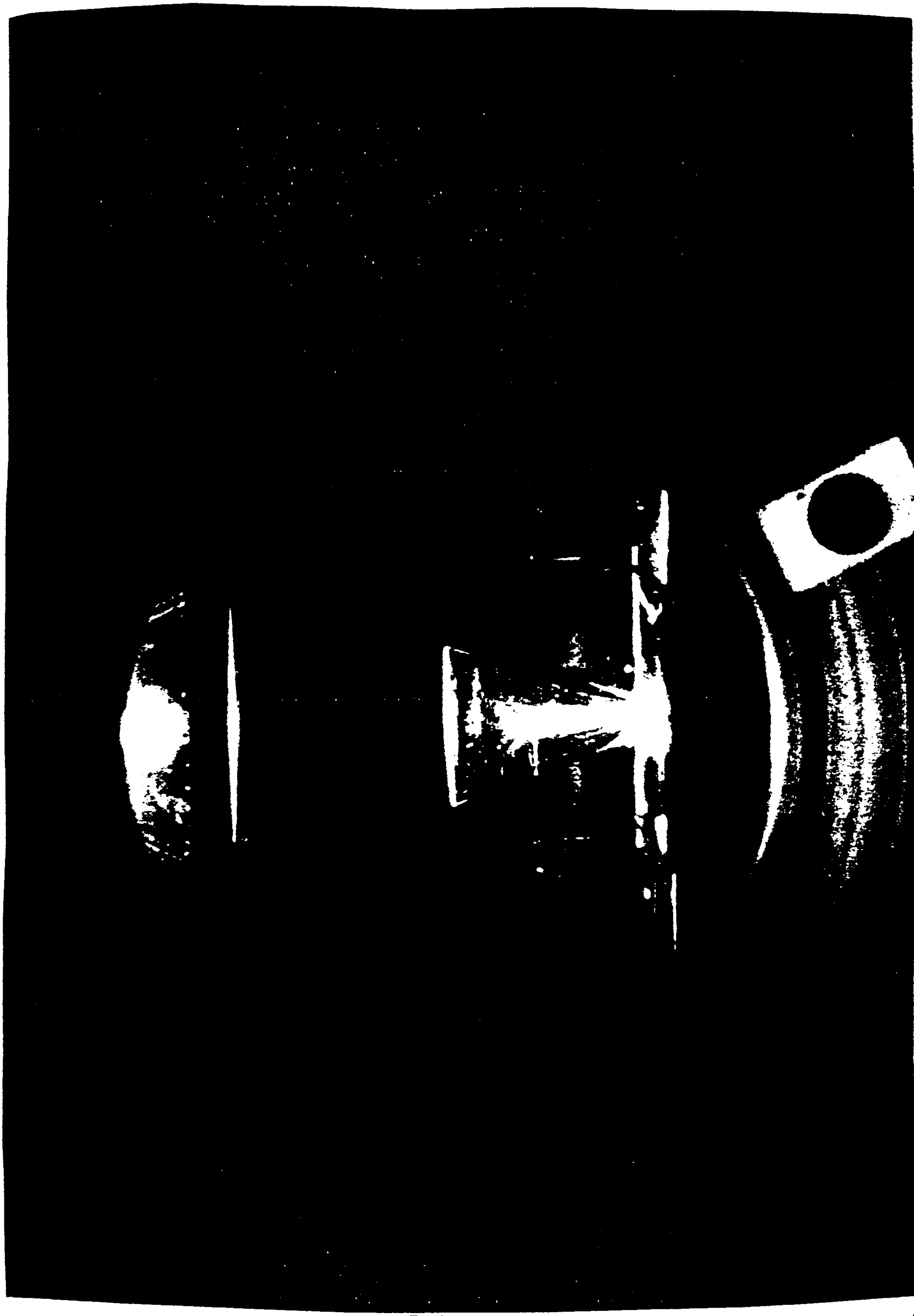

Figure 10-2. Light-Funnel Cell Assembly in Thermal Cycling Test Apparatus

SECTION 11.0

RADIATION TESTING

Radiation testing was conducted using 1-inch square by 0.020-inch thick type 7070 borosilicate glass samples. One sample was exposed to a fluence of 5×10^{15} e/cm^2 with 1.0 MeV electron energy. A second sample was exposed to a fluence of 1×10^{13} p/cm^2 with 0.8 MeV proton energy. Spectral transmission was measured before and after irradiation over the range from 350 nm to 900 nm. Figure 11-1 shows the results of these tests. No damage occurred for the proton exposure so the post-irradiation curve overlaps the pre-irradiation curve.

Other radiation tests have been conducted on various grades of fused silica. Charged particle radiation in some grades of fused silica tends to form absorption centers. Due to the relatively long pathlength of photons through the light funnel, such color centers would produce losses in efficiency of light transmission through the system. However, if high purity forms of fused silica such as Dynasil^R are used then tests have shown that it performs well after exposures to 2.7×10^{15} e/cm^2 (1.2 MeV) and 1×10^{11} p/cm^2 (3-4.6 MeV), respectively. These exposures are more than equivalent to many space missions. Further, UV radiation tends to bleach the absorption centers so that in real-time space applications, the radiation darkening of the light funnels should be negligible.

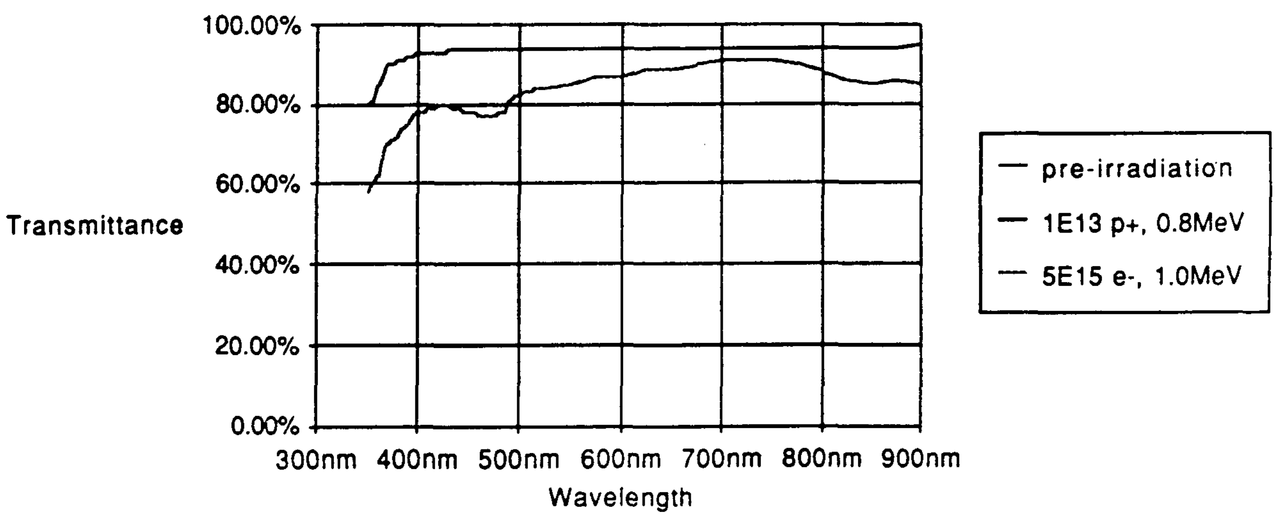

Figure 11-1. Radiation Effects on Spectral Transmittance

SECTION 12
CONCLUSIONS

12.1 LIGHT FUNNEL DIMENSIONS

The measured dimensions of the 12 light funnels manufactured for this program by Weiss Scientific Glass are presented in table 8-1 along with the design funnel dimensions. A graphical representation of the cone angle variation is shown in figure 8-1. Other significant deviations from the light funnel design included beaded cone lips of varying thicknesses as a result of the flame polishing finishing operation, and varying degrees of rounding of the inner cone apex. These distortions from the light funnel design caused large variations in the light funnel performance data.

The most significant parameters in correlating the light funnel performance data are the base diameter and the cone angles. The best performing light funnels, #3 and #10, both have relatively small base diameters and a similar angle difference between the inner and outer cone surfaces.

Light funnel s1 showed a much higher efficiency than the funnels of the initial design for a much higher concentration ratio. Major differences between the funnels were the extension of the inner cone down to the bottom surface and the surface finish. Funnel s1 was mechanicaly ground and polished rather that being formed by the heat process using a graphite wedge. Light funnel s1 was fabricated using fused silica grade 7940 rather than borosilicate glass grade 7740. The fused silica showed a much better transmittance than the borosilicate glass.

12.2 POINTING ANGLE

Concentrator output was quite tolerant to pointing angle error with a typical output of approximately 90% at 2 degrees off-normal. There were only slight variations observed between the x and y planes of angle measured. For some concentrators, the output was measured for angles extending to over 6 degrees with the level remaining above 60% of the maximum value. Use of the GaAs concentrating cell instead of the integrating sphere to measure output showed little change in sensitivity to pointing angle.

The measured pointing angle tolerance of the light funnels mounted to the GaAs solar cells exceeded the theoretical pointing angle tolerance of the design light funnel as illustrated in figure 12-1. While this high level of pointing angle tolerance would allow greater flexibility in array mounting methods, the pointing angle accuracy attained in a typical space application is within ±1 degree. The higher pointing angle tolerance is gained with the sacrifice of light funnel concentration performance, and the measured light funnel performance was less than predicted for the design funnel. This suggests a closer tolerance to the design light funnel dimensions is required to provide optimum light funnel performance.

12.3 ANTIREFLECTION COATINGS

Application of coatings did not have an appreciable effect on loss of output due to pointing angle error. The coatings did improve overall performance significantly. Typical improvements of 30% or greater were noted with the application of magnesium fluoride antireflection coatings. From the results, it appears that roughly half of the improvement came from the inner surface of the cone, and half from coating the base when measuring into the integrating sphere.

While the actual AR-coatings applied to the light funnels were not optimum, the light funnel performance improvement was greater than can be accounted for in surface reflectance reduction. A possible secondary effect of the AR-coatings is microscopic smoothing of the coated surfaces, which would reduce light scatter and improve light funnel efficiency. It is likely that further gains in light funnels performance would occur with an optimized AR-coating and smoother surface finishes.

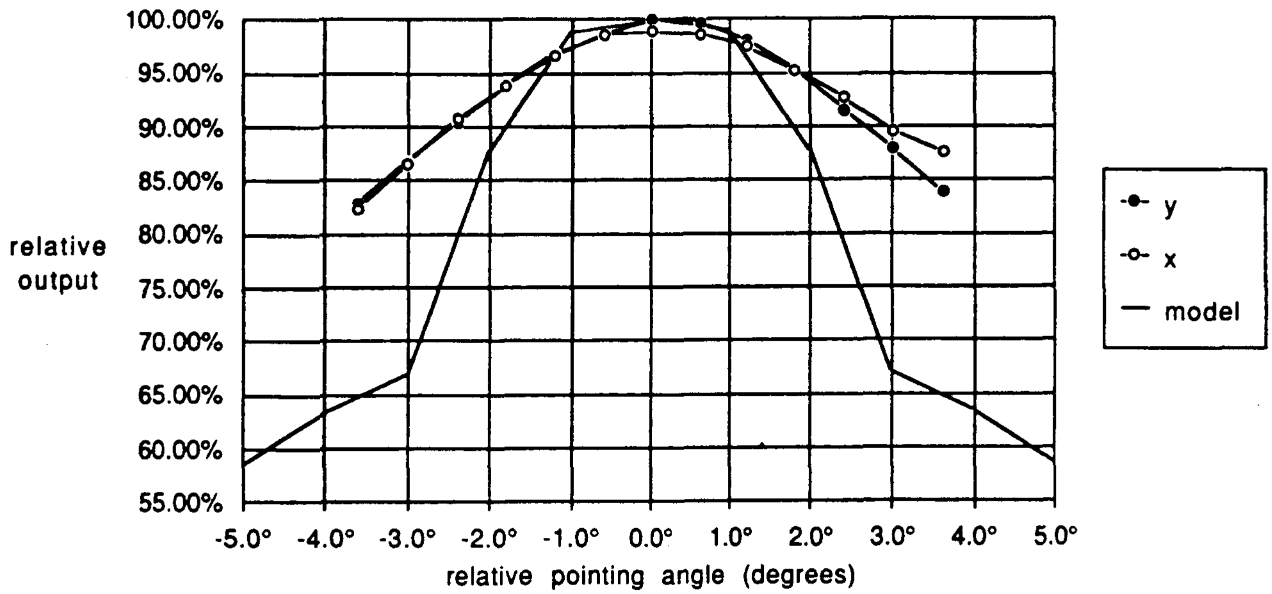

Figure 12-1. Light Funnel 10 on GaAs Cell

SECTION 13.0
RECOMMENDATIONS

13.1 MODELING

Performance improvements could be realized by further modeling of the light funnel design, particularly in the choice of wall angles and base configuration. Future models should take into account reflection from the surface of the concentrator cell. The effect of antireflection coatings should also be included. Modeling should be used to analyze the performance trade-offs between concentration ratio, weight, cell efficiency, and height.

13.2 FABRICATION

Fabrication techniques should be investigated to reduce concentrator costs and improve control over dimensions. Improved dimensional control is required in order to achieve consistently high concentration ratios and efficiencies. The models mentioned above should be used to predict and make trade-off choices in fabrication tolerances. Specifically, the relationship of tolerance allowed in the wall angle and the weight and concentration ratio should be modeled. In the same way the relation between the minimum wall thickness at the top of the funnel and the weight and concentration ratio needs to be reviewed. The material used needs to be fused silica or some other material that has a high transmittance for the thicknesses on the order of 3 cm.

13.3 AR-COATING

Further investigation into multilayer AR-coatings for the light funnel inner cone surface is recommended, since significant efficiency improvement could be gained by reducing the reflection of the inner cone. The drawback of the narrow wavelength range bandpass associated with multilayer coatings needs to be quantitatively compared to the improvement in light transmission. Further efforts to isolate the effects of AR-coatings from surface texture effects also would be helpful in understanding the light funnel efficiency losses.